energies

MDPI

Article

Heat Pumps and Optimized Thermal Management Strategies in Battery-Electric Rail Vehicles—Modeling and Evaluation

Steffen Wieser [1,*], Moritz Schenker [1], Linus Brünner [1] and Lutz Boeck [2]

[1] Institute of Vehicle Concepts, German Aerospace Center (DLR), Pfaffenwaldring 38-40, 70569 Stuttgart, Germany
[2] Wabtec Germany GmbH, 04435 Schkeuditz, Germany
* Correspondence: steffen.wieser@dlr.de

Abstract

Battery-electric rail vehicles are a sustainable alternative for diesel-powered vehicles on tracks without catenary. However, the energy demand to heat and cool the cabin limits the vehicle range, and the applied synthetic refrigerants are environmentally harmful. Therefore, this paper studies how energy demand and load on the battery in battery-electric rail vehicles can be reduced using heat pumps with natural refrigerants and efficient thermal management. A heat pump and thermal car body model are developed and validated, which calculate the energy demand in battery-electric rail vehicles. In these models, an optimized thermal management strategy is implemented, which changes the cabin set-point temperature based on catenary availability. For a two-car battery-electric rail vehicle in the climate zone II of Central Europe, the annual thermal energy demand is up to 110 MWh. The application of a heat pump with R290 (propane) can reduce the annual electrical energy demand for heating and cooling by up to 55%. The load on the battery can be mitigated further with the optimized thermal management strategy, reducing the equivalent full cycles by 3%. Overall, the heat pump operation and efficient thermal management strategy lead to higher vehicle range and flexibility in daily operation, increasing the acceptance of battery-electric rail vehicles.

Keywords: heating; air-conditioning; HVAC; natural refrigerants; cabin model; battery-electric rail vehicles; BEMU; battery trains; catenary-dependent thermal management; passenger transport

Academic Editor: Jan Taler

Received: 22 July 2026
Revised: 20 August 2026
Accepted: 23 August 2026
Published: 25 August 2026

1. Introduction—State-of-the-Art in Battery-Electric Rail Vehicles and Their Thermal Management Systems

Battery-electric rail vehicles are an emerging technology to enable sustainable rail transport. The following section introduces the operation of those vehicles and the different sub-systems and components. Additionally, the thermal management and systems for heating, ventilation, and air-conditioning (HVAC) are introduced, with a focus on natural refrigerants and heat pump operation. Based on this introduction and state-of-the-art analysis, the research question is concluded and presented at the end of the following section.

1.1. Battery-Electric Rail Vehicles: Operation and Components

The share of electrified rail tracks in the European Union (EU) is 57%. This means that 43%, or 85,000 km of the track network, is used by rail vehicles with an internal power supply [1]. For those vehicles, the state-of-the-art power supply is diesel, with 25,000 diesel-powered rail vehicles in operation in Europe [2]. Sustainable alternatives for the operation of vehicles on non-electrified track sections are battery-electric or hydrogen rail vehicles. Operating hydrogen rail vehicles presents challenges due to the high cost of hydrogen as an energy carrier. Further challenges include the need for a safe and fast refueling process for the large quantities of hydrogen required by rail vehicles [3]. The operation of battery-electric rail vehicles has challenges in providing sufficient range for the vehicles, based on the lower volumetric and gravimetric energy density of batteries compared to liquid energy carriers like diesel.

Battery-electric rail vehicles can switch between external power supply from catenary and internal power supply from the battery system. Thus, local trackside electrification with charging opportunities is a factor that determines the feasibility of battery-electric vehicles [4]. Optimization for these individual boundary conditions of the operation is also focused on the speed profiles or the internal power control of the vehicles [5]. In addition, it is challenging to provide sufficient range in operation due to the high energy demand to heat and cool the cabin for passengers, especially at very high or very low ambient temperatures [6].

In Germany, the operation of battery-electric rail vehicles started in 2023 with battery-electric multiple units (BEMU) for passenger transport [7]. Since then, different networks have adopted the operation of these vehicles or will start them in the next few years. Exemplary BEMU fleets are the NAH.SH network with 55 vehicles, Niederrhein-Münsterland network with 66 vehicles or Ostbrandenburg network with 31 vehicles [8]. In other European countries, the adaptation of battery-electric rail vehicles has started as well. Overall, around 600 battery trains have already been ordered in Europe [9]. Globally, the number of networks and projects with battery-electric rail vehicles has been increasing, particularly in Asia and North America.

The vehicles used in the mentioned rail networks are regional rail vehicles, not high-speed trains, as the tracks for high-speed trains are mainly electrified due to high energy demand. Regional rail vehicles with batteries are, for example, the Alstom Coradia Continental BEMU, CAF Civity BEMU, Siemens Mireo Plus B, and the Stadler FLIRT AKKU. These vehicles have a length of about 40 m to 50 m, resulting in a seating capacity of about 100 to 150 seats. The maximum speed is between 140 km/h and 160 km/h, and the range in battery operation is stated to be between 80 km and 120 km. The power- and energy-related components in the vehicles include batteries, power electronics, and e-motors [10]. The battery system is used as an on-board energy storage system (OESS) with a capacity between 500 kWh and 1000 kWh [11]. Lithium-titanium-oxide (LTO) batteries are mainly used in rail vehicles because they are safer and enable more cycles over their lifetime compared to lithium nickel manganese cobalt oxide (NMC) and lithium iron phosphate (LFP) batteries [12]. The cycling of the batteries is measured in equivalent full cycles (EFCs), where one EFC is equivalent to one complete charge and discharge of the overall battery capacity [13]. The cycling and aging of the battery cells is important for the operation of rail vehicles, as it affects reliability, maintenance effort and costs over a vehicle lifetime of up to 30 years. Therefore, opportunities for reduced battery cycling are part of current research [14]. In track sections without catenary, the electrical power from the battery is provided to the direct current (DC) link with DC/DC converters. In sections with catenary, the electrical power for the DC-link is supplied by a pantograph and a transformer. DC-to-alternating-current (AC) inverters provide electrical power from the DC-link to the traction e-motors, which transform electrical energy into mechanical energy to move the

https://doi.org/10.3390/en19173990

vehicles. Additionally, DC/AC inverters provide the electrical power for auxiliaries such as lights, passenger information systems, and HVAC systems [10].

Overall, it becomes clear that battery-electric rail vehicles are a rising technology for operation on partly-electrified track sections, as more of these vehicles are available from vehicle manufacturers and are in operation in several regional rail networks. The current challenges deal with the lifetime of the battery systems and sufficient range in operation.

1.2. Rail Vehicle Thermal Management and HVAC Systems

Thermal management in rail vehicles includes the heating and cooling of all power components [15]. For battery-electric rail vehicles, this includes the battery, power electronics, e-motors, and the HVAC system for the cabin. Specifically, the combination of battery and cabin thermal management is a major part of current research [16]. The temperature in the cabin of regional rail vehicles is controlled based on set-point temperature values from EN 14750 [17]. The temperature inside the cabin needs to stay within an interval between minimum and maximum cabin temperature, which depends on the ambient temperature [18]. For relatively higher ambient temperatures, the cabin temperature is higher to limit energy demand by reducing the temperature difference between ambient and cabin for the passengers. The thermal management in rail vehicles also depends on the environmental conditions of operation, which are defined in EN 50591. EN 50591 includes a standardized calculation of energy demand in rail vehicles. One part of this calculation considers energy demand for cabin heating and cooling based on standardized operating points for regional vehicles. Specified parameters include ambient temperature, humidity, and annual working hours [19]. Thermal comfort parameters for these calculations are taken with reference to EN 14750 and EN 13129 [60]. These operating conditions strongly affect the energy demand of the HVAC system. Over a full year of operation, up to 30% of the overall energy demand of the vehicle is for the HVAC system [20]. In a use case in Germany, this corresponds to 30 MWh of annual energy to heat or cool the cabin [21]. This implies that comfort functions and the HVAC system provide opportunities to reduce energy demand for the vehicles in operation [22]. In addition to the temperature in the cabin, humidity needs to be considered in the vehicle energy demand, as dehumidification increases energy demand at high ambient temperatures [23].

For the investigation of thermal comfort and temperature distribution in the vehicle, computational fluid dynamics (CFD) models and simulations are used [24]. For investigations focused on energy demand in rail vehicle operation, lumped-parameter models are used, which have sub-models for heat transfer through cabin walls and conditioning of cabin air flows [25]. Multi-zone models can be used for a level of detail between CFD and lumped-parameter models [26]. In all these models, the HVAC system and the respective cabin temperature and humidity control are abstracted.

HVAC systems for rail vehicles are often placed on the roof of the vehicles and have a higher nominal power level compared to road vehicles, as the cabin is larger. At least one HVAC system is installed per car, which leads to several HVAC systems in a complete rail vehicle. HVAC systems for the driver and passengers are separated from each other. Passenger cabin systems have a nominal power level between 10 kW and 60 kW, and the driver cabin systems are around 5 kW [27]. The systems suck in fresh air from the environment and circulating air from the cabin to create a mixed air flow. The mixed air flow is cooled or heated in the HVAC system and guided to the cabin in ventilation ducts. Inside the cabin, there are additional electrical resistance heaters that support the heating system at low ambient temperatures. In future battery-electric rail vehicles, thermal storage systems may be used as part of the thermal management system to provide an additional heat source [28]. Currently, HVAC systems consist of resistance heaters, a refrigerant compressor, an expansion valve, and heat exchangers, and the behavior of all these

https://doi.org/10.3390/en19173990

components affects the HVAC energy demand [29]. In the vapor compression cycle, different refrigerants are used to cool the air for the cabin. According to Trygstad et al. [30], 75% of HVAC systems in rail vehicles use R134a as a refrigerant and 25% use R407C. R410A is also used in some rail vehicles [31]. R1234yf is studied for rail vehicle application as well, but has similar performance values compared to R134a [32].

In general, thermal management and HVAC systems in rail vehicles have a substantial share in the vehicle energy demand because of the large cabin. Resistance heaters are the established technology for heating, whereas vapor compression cycles with synthetic refrigerants like R134a are established for cooling.

1.3. Heat Pumps and Natural Refrigerants in Rail Vehicles

The vapor compression cycle can be used in an air conditioner to cool the ambient air by absorbing heat in the evaporator. Heat pumps use the same cycle to provide heat to the ambient air at the condenser. Therefore, heat pumps can be used as a heat source in several applications. Industrial processes are especially beneficial for the applications of heat pumps, as fewer changes in the aimed heating temperature of the working fluid are expected compared to household systems [33]. Industrial processes also use working fluids from the processes as heat sources for the heat pump. In mobile applications, such as automotive battery-electric passenger cars, air-source heat pumps are applied to use ambient air as a heat source. Scroll compressors are used as compressor technology for these mobile heat pump applications [34]. Furthermore, the vapor compression cycle is not only used to provide thermal comfort in the cabin but also in the thermal management of batteries in an integrated vehicle thermal management system [35]. R134a is an established refrigerant for heat pumps in passenger cars, but systems with R290 (propane) and R744 (CO_2) are also entering the market [36]. For these new refrigerants, optimization methods for heat pumps in mobile applications have been studied, e.g., machine-learning-based optimizations to increase heat transfer at gas coolers [37]. Given these references, it becomes clear that heat pumps are an emerging technology in stationary and mobile applications.

Also, in regional and urban rail vehicles, heat pumps are a key technology in reducing energy demand [38]. In the heat pump process, the refrigerant is compressed in the compressor, which also increases the temperature of the refrigerant. The hot refrigerant is guided through the condenser heat exchanger, where it heats up the air for the cabin. Afterwards, the refrigerant expands in the expansion valve, leading to a temperature reduction in the refrigerant. The cold and liquid refrigerant flows through the evaporator heat exchanger and absorbs heat from the ambient air, leading to evaporation of the refrigerant. This closes the loop in the heat pump process as the refrigerant is then compressed again. A key performance indicator for heat pumps is the coefficient of performance (COP). The COP is the ratio between thermal energy provided to the air for the cabin and the electrical energy for the HVAC system. For refrigeration systems, this ratio is called EER (energy efficiency ratio). For simplification, the COP is used for heating and cooling in this study. The ideal COP, based on the vapor compression cycle, differs from the real COP measured in rail vehicles because of the efficiency of components like the compressors and fans for heat exchangers and ventilation. A ratio between the Carnot COP and real COP of 0.225 is stated by Deutsche Bahn, according to Donner et al. [39], based on empirical evaluation. Constant COPs are applied for simplification in some studies about rail vehicles. For example, in Xu et al. [40], a COP of 3 is stated for the investigation. More detailed approaches analyze the heat pump COP as a function of the ambient temperature. The COP decreases with greater temperature differences between cabin and ambient temperatures. This leads to measures like vapor injections, which are applied to increase heat pump COP at low ambient temperatures [41]. Vapor injection technology

https://doi.org/10.3390/en19173990

provides an increase in the COP from 1 to 1.6 at −25 °C ambient temperature [42]. In addition to temperature, the ventilation strategy also affects the COP of heat pumps in vehicle applications [43].

Several manufacturers of HVAC systems for rail vehicles develop and offer heat pump systems. Wabtec developed an R290 heat pump system for rail vehicles with technology readiness level 9 (TRL) [44]. Knorr–Bremse developed a system with R744 [45]. Liebherr developed heat pump systems with R290 and R744 [46]. The systems show power levels of around 20 kW and COP values between 1.5 and 4. R290 and R744 are used as natural refrigerants compared with synthetic ones like R134a introduced in the previous Section 1.2. Synthetic refrigerants need to be replaced, as they have a high global warming potential (GWP). The GWP of R134a is 1430. R1234yf has a lower GWP of 0.5 but degrades to trifluoroacetic acid (TFA) and is part of the per- and polyfluoroalkyl substances (PFAS), which could be restricted by EU regulation 2024/073 [47]. PFAS are restricted, as they are long-lasting chemicals that accumulate in the human body and pollute the environment. R1234yf is widely used in passenger cars, but very rarely in rail vehicles, so it is not further considered in this study. PFAS restrictions and the high global warming potential of synthetic refrigerants mean that future heat pump systems will use natural refrigerants.

The natural refrigerants R290 and R744 present additional challenges in their implementation in vehicles. Available heating power at low ambient temperatures with R290 is lower than with R744, if compressors are designed for refrigeration only [48]. R290 is flammable, which could pose a safety risk for passengers. This requires detailed safety assessments and measures. Dual-loop systems can be used with R290, so that there is no heat exchanger between R290 and the air transferred to the cabin. Small leakages in this heat exchanger could lead to a flammable atmosphere in the cabin. However, dual-loop systems lead to a loss in energy efficiency. In Kwon et al. [49], the COP in a single-loop system is between 8.3% and 49.5% higher, depending on the operating conditions. For dual-loop systems, a reconfigurable dual-core R290 vehicular thermal management system featuring a variable-area thermal unit can be used to overcome performance loss at high thermal loads [50]. R744 has a low critical point but needs to be operated at high temperatures, leading to transcritical operation. The components in the system need to be more robust to be compatible with this pressure. Risks of transcritical operation can be prevented with a liquid-state pressurized carbon dioxide ejector heat pump [51]. In passenger car operation, R744 heat pumps show a COP between 1 and 2.8 [52]. For rail vehicles, a COP between 1 and 4 is presented for ambient temperatures between 0 °C and 20 °C [53]. The amount of refrigerant needed in rail vehicles with R744 heat pumps is between 2.8 kg and 3.8 kg [54]. The amount of refrigerant per HVAC system is around 2.8 kg with R290, 9.6 kg with R134a, and 8.0 kg with R407C, according to Boeck et al. [44] and Zhang et al. [55]. The evaporator and condenser temperatures can differ between refrigerants, even though similar temperatures should be considered for reasons of efficiency. R744 systems are designed, for example, with a heat exchanger outlet temperature of 35 °C and an evaporation temperature of 5 °C in transcritical operation, whereas R290 systems are designed, for example, with a condenser outlet temperature of 45 °C and an evaporation temperature of 0 °C, according to Kwon et al. [56]. Another natural refrigerant for rail vehicles is air (R729), but HVAC systems with air have a lower COP than R290 and R744 systems [57].

Overall, it becomes clear that heat pump operation in rail vehicles needs to be based on natural refrigerants to contribute to sustainable transport. R290 and R744 are suitable natural refrigerants but offer different efficiencies in operation. As efficiency varies greatly with ambient conditions, a variety of operating conditions need to be considered for evaluation of heat pump systems in rail vehicles.

https://doi.org/10.3390/en19173990

1.4. Aims of This Study and Work Novelty

Efficient thermal management in battery-electric vehicles is a key research topic, as energy demand and battery degradation are strongly dependent on it. Thermal management systems with heat pumps and several refrigerants are discussed in the literature to control temperature levels in the cabin and other components. Heat pumps increase the energy efficiency compared to resistance heaters but require the use of natural refrigerants for sustainable heating in vehicles. Synthetic refrigerants are less sustainable because of their high GWP and their degradation to PFAS. For rail vehicles, heating, ventilation, and air-conditioning systems with natural refrigerants have been developed in recent years. However, studies demonstrating how these systems affect the energy demand and cycling of batteries in battery-electric rail vehicles represent a research gap. Additionally, strategies for the optimized operation of these systems with rail-specific boundary conditions are missing in the literature, as most studies about battery-electric mobility focus on passenger cars. Therefore, the presented work poses the research question: How do heat pumps with natural refrigerants and an efficient thermal management operating strategy affect energy demand and load on the battery in battery-electric rail vehicles? Accordingly, this work aims to present the effects of heat pumps and optimized thermal management strategies on daily operation. Additionally, it aims to present the effects of several climate zones and conditions and how they affect energy demand and battery cycling on an annual basis.

2. Methodical Approach—Modeling of Thermal Management in Battery-Electric Rail Vehicles

The following section presents the methodological research approach. A thermal car body and heat pump model are introduced and validated to calculate the energy demand for heating and cooling in a battery-electric rail vehicle. In addition, the parameter sets studied for battery-electric rail vehicle operation scenarios are introduced, including environmental conditions, track sections, and vehicle parameters.

2.1. Thermal Car Body Model: Structure and Variables

A thermal car body model (TCBM) was developed in Python 3.12 to calculate the thermal energy demand for HVAC systems in battery-electric rail vehicles. The TCBM developed and applied in this study is based on the model described in previous work [28]. The TCBM includes thermal modeling of the cabin and pre-conditioning of the air by the HVAC system, as visualized in Figure 1.

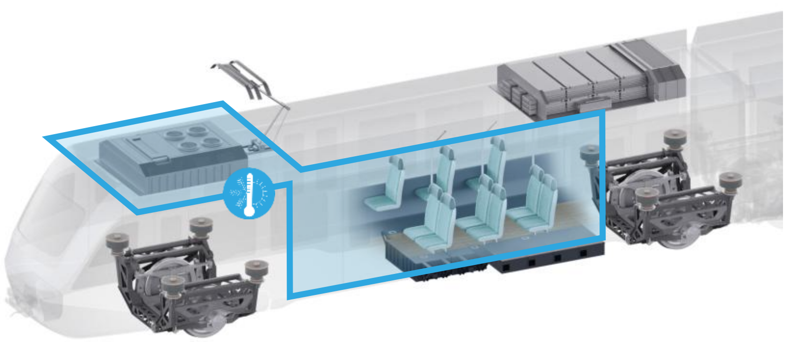

Figure 1. Schematic scope of the thermal car body model.

As a core principle of the TCBM, the first law of thermodynamics is set up in Equation (1).

$$\frac{dH}{dt} = \dot{Q}_{Trp} + \dot{Q}_{Rad} + \dot{Q}_{Pass} + \dot{Q}_{El} + \dot{m}_{in} \cdot h_{in} + \dot{m}_{Pass} \cdot h_{Pass} - \dot{m}_{out} \cdot h_{out} \tag{1}$$

The change in absolute enthalpy of the cabin air over time $\frac{dH}{dt}$ is calculated as the sum of the heat transported through the walls of the cabin $\dot{Q}_{Trp}$, the heat from solar radiation $\dot{Q}_{Rad}$, the heat emitted from the passengers $\dot{Q}_{Pass}$, the heat from electrical heat sources in the cabin $\dot{Q}_{El}$, as well as the mass flow of the air $\dot{m}_{Pass/in/out}$ and enthalpy $h_{Pass/in/out}$ emitted from passengers and of the air entering and leaving the cabin by ventilation.

The change in specific enthalpy of air in the cabin between two time steps Δh_{cb} is calculated in Equation (2) based on the mass of air in the cabin m_{cb}, the change in absolute enthalpy of the cabin air $\frac{dH}{dt}$, and the time step Δt. The specific enthalpy of the air in the cabin $h_{cb,t+1}$ is calculated in Equation (3) by adding the change in specific enthalpy Δh_{cb} to the specific enthalpy in the current time step $h_{cb,t}$.

$$\Delta h_{cb} = \frac{1}{m_{cb}} \cdot \frac{dH}{dt} \cdot \Delta t \tag{2}$$

$$h_{cb,t+1} = h_{cb,t} + \Delta h_{cb} \tag{3}$$

For the calculation of humidity, the change in mass of water in the cabin $\frac{dm_{w,cb}}{dt}$ is calculated in Equation (4) by summing up the mass of water entering and leaving the cabin based on air mass flows $\dot{m}_{in/out}$, the water emitted by passengers $\dot{m}_{Pass}$, and absolute humidity $x_{in/out}$ of the air entering and leaving the cabin by ventilation. The amount of water emitted by passengers $\dot{m}_{Pass}$ is calculated in Equation (5) based on the latent heat flow emitted from passengers $\dot{Q}_{Pass,lat}$ and the enthalpy of vaporization h_v. The change in absolute humidity in the cabin between two time steps Δx_{cb} is calculated in Equation (6) based on the mass of air in the cabin m_{cb}, the change in mass of water $\frac{dm_{w,cb}}{dt}$, and the time step Δt. The absolute humidity of the air in the cabin $x_{cb,t+1}$ is calculated in Equation (7) by adding the change in absolute humidity Δx_{cb} to the absolute humidity in the current time step $x_{cb,t}$.

$$\frac{dm_{w,cb}}{dt} = \dot{m}_{in} \cdot x_{in} + \dot{m}_{Pass} - \dot{m}_{out} \cdot x_{out} \tag{4}$$

$$\dot{m}_{Pass} = \frac{\dot{Q}_{Pass,lat}}{h_v} \tag{5}$$

$$\Delta x_{cb} = \frac{1}{m_{cb}} \cdot \frac{dm_{w,cb}}{dt} \cdot \Delta t \tag{6}$$

$$x_{cb,t+1} = x_{cb,t} + \Delta x_{cb} \tag{7}$$

Heat transfer equations in the model include the effects of conduction, convection, and radiation on the thermal behavior of the car body. The change in wall temperature $\frac{dT}{dt}$ is calculated in Equation (8) based on the heat flow from conduction at the inner and outer wall $\dot{Q}_{Cond,i/o}$ and the thermal capacity of the wall C. The wall temperature at the next time step T_{t+1} is calculated in Equation (9) by adding the change in temperature to the temperature in the current time step T_t. The energy balance for the wall itself sums up all heat flows from conduction inside and outside $\dot{Q}_{Cond,i/o}$, convection inside and outside $\dot{Q}_{Conv,i/o}$, and absorbed and emitted radiation $\dot{Q}_{Rad,abs/em}$ in Equation (10). Heat flow from conduction $\dot{Q}_{Cond,i/o}$ is calculated in Equation (11) based on thermal conductivity λ, wall area A, wall thickness d, as well as the temperature difference between inside the wall T and the surface $T_{Surf,i/o}$. Heat flow from convection $\dot{Q}_{Conv,i/o}$ is calculated in

Equation (12) based on the heat transfer coefficient $\alpha_{i/o}$, wall area A, as well as the temperature difference between the surface of the wall $T_{Surf,i/o}$ and the temperature in the cabin or ambient $T_{cb/amb}$. Heat transfer coefficients at the outside of the wall α_o are calculated in Equation (13) separately for walls and windows depending on the vehicle velocity v. Overall, the energy balance for the wall can be rearranged to yield the wall surface temperature $T_{Surf,i/o}$ in Equation (14).

$$\frac{dT}{dt} = \frac{\dot{Q}_{Cond,i} + \dot{Q}_{Cond,o}}{C} \tag{8}$$

$$T_{t+1} = T_t + \frac{\dot{Q}_{Cond,i,} + \dot{Q}_{Cond,o}}{C} \cdot \Delta t \tag{9}$$

$$\dot{Q}_{Cond,i/o} = \dot{Q}_{Conv,i/o} + \dot{Q}_{Rad,abs} - \dot{Q}_{Rad,em} \tag{10}$$

$$\dot{Q}_{Cond,i/o} = \frac{2\,\lambda}{d} \cdot A \cdot (T_{Surf,i/o} - T) \tag{11}$$

$$\dot{Q}_{Conv,i/o} = \alpha_{i/o} \cdot A \cdot (T_{cb/amb} - T_{Surf,i/o}) \tag{12}$$

$$\alpha_{o,window} = \begin{cases} 5{,}6 + 4 \cdot v \\ 7{,}12 \cdot v^{0{,}78} \end{cases} \alpha_{o,wall} = \begin{cases} 5{,}8 + 4 \cdot v & for\ v < 5\ \mathrm{m/s} \\ 7{,}14 \cdot v^{0{,}78} & for\ v \geq 5\ \mathrm{m/s} \end{cases} \tag{13}$$

$$T_{Surf,i/o} = \frac{\frac{2\,\lambda}{d} \cdot A \cdot T + \alpha_{i/o} \cdot A \cdot T_{amb/cb} + \dot{Q}_{Rad,abs} - \dot{Q}_{Rad,em}}{(\frac{2\,\lambda}{d} + \alpha_{i/o}) \cdot A} \tag{14}$$

Similar calculations are performed for the wall and window areas of the car body, taking into account that radiation is transmitted for window areas and absorbed at the surface for wall areas. All volume flows $\dot{V}$ and heat flows $\dot{Q}$ relevant for evaluating the energy balance of the cabin in the TCBM are summarized in Figure 2.

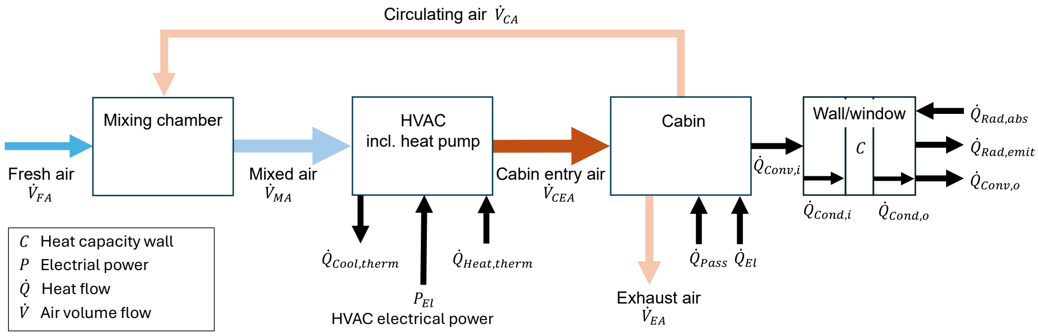

Figure 2. Schematic scope of the thermal car body model including heat and air volume flows and heat pump model (updated from [28]).

In addition, the HVAC COP model is given, which determines electrical energy demand based on the thermal energy demand calculated by the TCBM. The TCBM is connected with a simulation pipeline to the pySimRail vehicle model developed at DLR to study the effects of the calculated energy demand for HVAC systems on the vehicle level [58]. The pySimRail vehicle model simulates the driving dynamics of the rail vehicle based on a timetable and determines power profiles at all relevant components of the vehicle energy management.

2.2. Heat Pump Model: Structure, Variables and Operating Strategy

A COP model was developed in Python to determine the electrical energy demand for HVAC systems with heat pumps in battery-electric rail vehicle operation. The calculation of the ideal COP (COP_{ideal}) is performed according to Equation (15) for heating operation as a heat pump, and according to Equation (16) for cooling operation as an air conditioner. The COP is defined as the relation between heat at condenser Q_{cond} or evaporator Q_{evap} and the work of the compressor W_{comp}. These depend on the specific enthalpy of the refrigerant after evaporator h_1, compressor h_2, condenser h_3 and expansion valve h_4. The calculated ideal COP is based on the simple saturated cycle, which is assumed without any superheating or sub-cooling, as presented in the log(p)-h-diagram in Figure 3.

$$COP_{ideal,heat} = \frac{Q_{cond}}{W_{comp}} = \frac{h_2 - h_3}{h_2 - h_1} \quad (15)$$

$$COP_{ideal,cool} = \frac{Q_{evap}}{W_{comp}} = \frac{h_1 - h_4}{h_2 - h_1} \quad (16)$$

The specific enthalpy of the refrigerant after the evaporator h_1 is given in Equation (17) based on the temperature at the evaporator T_{evap} and the saturation pressure at this temperature $p_{sat,Tevap}$, as the refrigerant is assumed to be in the state of saturated steam. A visualization of the vapor compression cycle with the corresponding components and states of refrigerant is presented in Figure 3 in a component overview and log(p)-h-diagram.

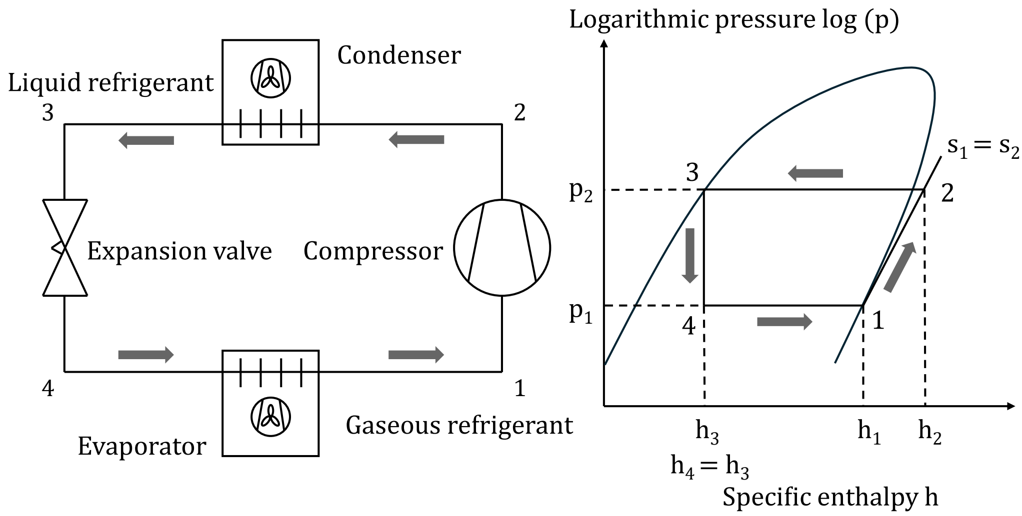

Figure 3. Vapor compression cycle components (**left**) and log(p)-h-diagram with the four different states of the refrigerant during the cycle (**right**).

The specific enthalpy of the refrigerant after the compressor h_2 is given in Equation (18) based on the assumption of isentropic compression and the saturation pressure at condenser temperature $p_{sat,Tcond}$. The specific enthalpy of the refrigerant after the condenser h_3 is given in Equation (19) based on the temperature at the condenser T_{cond} and the saturation pressure at condenser temperature $p_{sat,Tcond}$. The specific enthalpy of the refrigerant after the expansion valve h_4 is set equal to h_3 in Equation (20) based on the isenthalpic expansion at the expansion valve. All states and specific enthalpies of the refrigerant are determined by solving the fundamental Helmholtz energy equations of state in CoolProp 6.6.0 [59].

$$h_1 = h_1(T_{evap}, p_{sat,Tevap}) \tag{17}$$

$$h_2 = h_2(s_1 = s_2, p_{sat,Tcond}) \tag{18}$$

$$h_3 = h_3(T_{cond}, p_{sat,Tcond}) \tag{19}$$

$$h_4 = h_3 \tag{20}$$

The calculation of the COP based on the ideal vapor compression cycle relies on ideal assumptions and lacks information to calculate the electrical energy demand of HVAC systems with heat pumps in rail vehicle operation. A factor f_{COP} = 0.4 was determined to define the ratio between ideal and real COP and is based on a value from German rail operator Deutsche Bahn in Donner et al. [39]. It describes the ratio between the COP from the ideal vapor compression cycle COP_{ideal} and the real COP (COP_{real}) based on the electrical energy demand of HVAC systems appearing in rail vehicle operation, as stated in Equation (21). The factor takes into account the losses as well as the electrical energy demand for fans and other components in the HVAC system.

$$COP_{real} = f_{COP} \cdot COP_{ideal} \tag{21}$$

Based on the heat pump and refrigeration model, the COP values are determined for different ambient temperatures and refrigerants, as presented in Figure 4. R134a is presented as a widely applied synthetic refrigerant in comparison to the natural refrigerants R290 and R744. The COP curves for heating are presented to the left in Figure 4, down to an ambient temperature of −40 °C. All heating mode curves are calculated with a condenser temperature between 30 °C and 40 °C. The evaporator temperature in heating mode is set 10 K colder than the ambient temperature. R744 shows a lower COP compared with R134a and R290, and the COP is less than 1 for R744 below −25 °C.

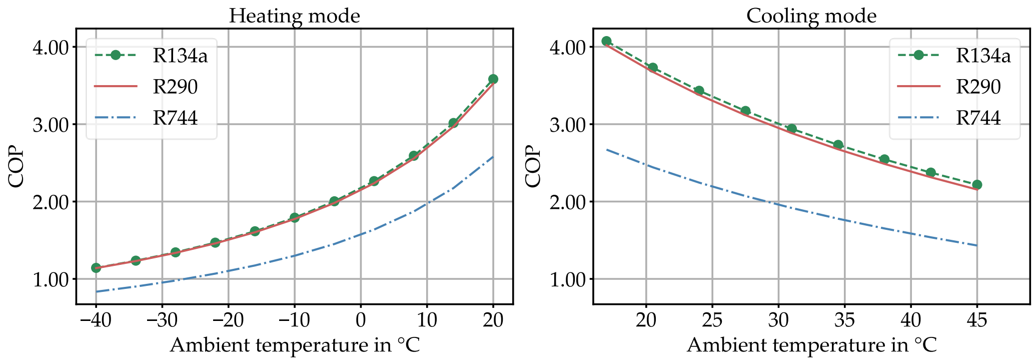

Figure 4. Modeled COP curves for heating (**left**) and cooling (**right**) with different refrigerants.

The COP curves for cooling are presented to the right in Figure 4 up to an ambient temperature of 45 °C. Curves are calculated with an evaporator temperature between 0 °C and 15 °C. The condenser temperature in cooling mode is set 10 K higher than the ambient temperature. Similar to the COP curves for heat pump mode, the COP for R744 is lower than for R134a and R290. For R744 at temperatures higher than 30 °C, the vapor compression cycle turns into a transcritical cycle where the refrigerant operates above its critical point. The developed heat pump model is not designed for transcritical fluid modeling, so for transcritical operation, the R744 COP is extrapolated based on the subcritical COP and the ratio to the COP of R290. Overall, the COP values for the three studied refrigerants vary from 0.8 to 4.1 over heating and cooling modes combined.

In addition to the ambient temperature, the energy demand for heating and cooling is highly dependent on the temperature in the cabin. The higher the temperature difference between cabin and ambient, the higher the energy demand for the HVAC system. Set-point curves for the cabin temperature in regional rail vehicles are defined in DIN EN 14750 [18]. For every ambient temperature, upper, lower, and recommended set points for the cabin temperature are stated in the corresponding set-point curves. The difference between upper and lower set-point temperatures gives a degree of freedom in the operation of the vehicles while maintaining thermal comfort for the passengers. Based on these boundary conditions, an optimized thermal management strategy for battery-electric rail vehicles is developed and presented in Figure 5.

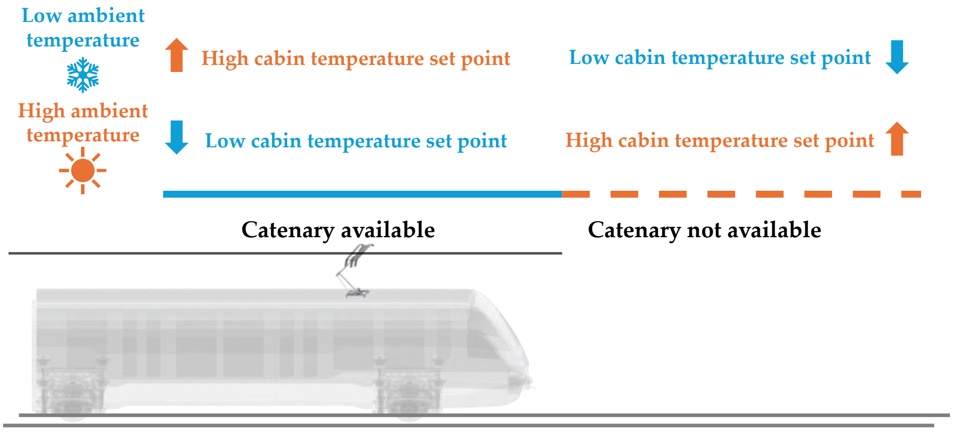

Figure 5. Optimized thermal management strategy based on set-point temperatures for the cabin depending on catenary availability.

The aim of the optimized thermal management strategy is to minimize energy demand for the HVAC system provided by the battery. Therefore, in track sections where catenary is not available, the set-point temperature in the cabin is set to the upper limit for cooling cases and to the lower limit for heating cases. As soon as the catenary is available, the set-point temperature switches to the lower limit for cooling cases and the upper limit for heating cases. This increases energy demand in sections with catenary but also conditions the cabin thermally to reduce energy demand even further in the next section without catenary.

2.3. Validation of Simulation Models

The simulation results from the presented models are compared to measurement values to validate the results. For the validation process, measurement data from rail vehicles in operation is used. The electrical power demand on HVAC systems is measured, as well as the ambient and cabin temperatures. Time intervals of the same length are chosen from the measurement data, and the HVAC power is cumulated to an HVAC energy demand over the whole interval. The measured electrical HVAC energy demand in comparison to the simulated energy demand is presented in Figure 6. The HVAC systems in the measured vehicles are operated with discrete power steps, which means that the power deviates over time compared to the simulated power values from the TCBM.

The comparison of the cumulated energy values helps to remove the effects of the individual operation strategy and focuses the validation process on the overall energy balance. Six different ambient temperatures are evaluated from cold conditions at −5 °C up to hot conditions at 34 °C. The measured energy demand is between 4 kWh and 29 kWh, whereas the simulated energy demand is between 4 kWh and 22 kWh. The highest energy demand occurs, as expected, at the lowest and highest ambient temperatures. The measured values include some effects of the environment that are not available in the measurement data, such as solar radiation and wind velocity. For these effects, assumptions are made in the simulation. Solar radiation is assumed to be 0 W/m² in the heating cases and 400 W/m² in the cooling cases. Wind velocity is assumed to be 0 km/h for a parked vehicle. The uncertainty in the measurement data concerning these effects explains the range of different values for the energy demand at the same temperature.

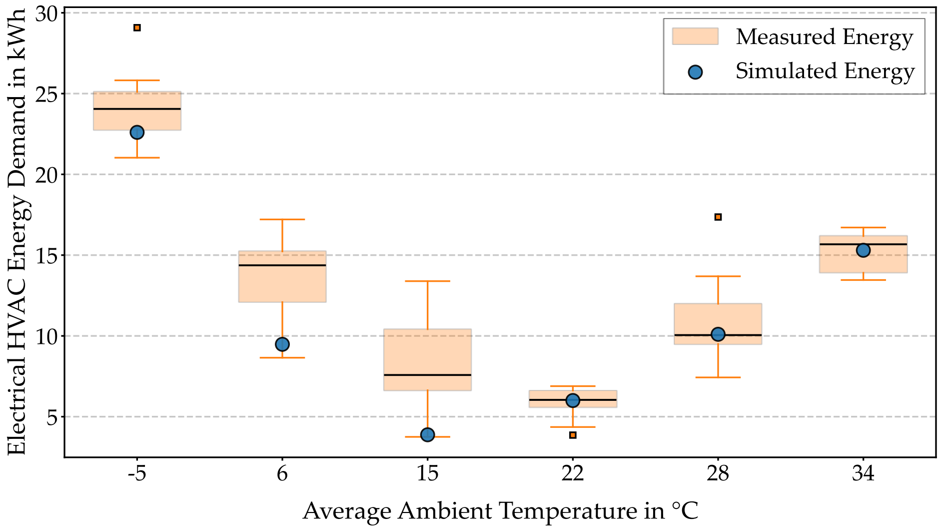

Figure 6. Comparison between simulated and measured HVAC energy demand at different ambient temperature levels.

Several measurement data sets at the same average ambient temperature are analyzed to identify the range of values for the electrical HVAC energy demand at this temperature. For most cases, the simulated energy demand is lower than the measured one. In the case with the highest ambient temperature, the simulated energy demand is higher than the measured value. This can be explained by the fact that the mechanical dehumidification implemented in the model generates high energy demand. In a qualitative comparison, the results show that the simulation results for different operating points are similar to the measured energy demands. This supports the conclusion that the models provide reliable results for HVAC energy demand. The models are therefore validated and suitable for investigating the effects of heat pumps and an optimized thermal managemsectionent strategy on the operation of battery-electric rail vehicles.

2.4. Use Case Scenarios and Parameter Sets of Battery-Electric Rail Vehicle Operation: Vehicle, Tracks and Climate Zones

To study different refrigerants in heat pumps and efficient operating strategies in battery-electric rail vehicles, suitable parameter sets for environmental conditions, track, vehicle and HVAC control are specified. These parameter sets are used as input for the TCBM to generate the results presented in Section 3.

For the environmental conditions, several rail-specific standards such as EN 14750 and EN 13129 define different climate zones for operation in Europe, as presented in Figure 7. Each country is assigned a climate zone from I to III in summer and winter. Southern Europe is defined with climate zone I, Central Europe with climate zone II and Northern Europe with climate zone III in both seasons. In general, climate zone I is characterized by higher ambient temperatures and climate zone III by lower ambient temperatures. Most countries are assigned the same climate zone for summer and winter, but Great Britain, Poland, and Italy, for example, have different climate zones in winter and summer.

https://doi.org/10.3390/en19173990

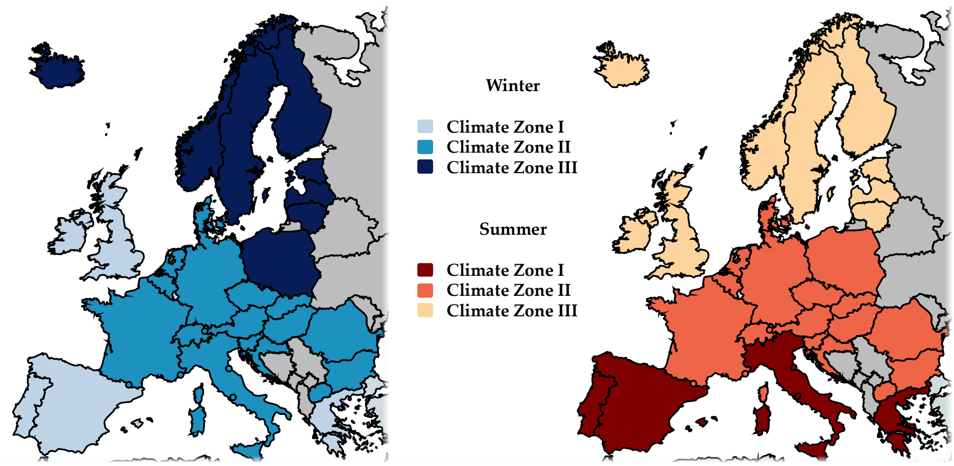

Figure 7. Climate zones of operation for regional rail vehicles according to EN 14750 [18] and EN 13129 [60] (maps created with [61]).

Assigned climate zones lead to different standardized operating points (OP) for rail vehicles, according to EN 50591, as presented in Table 1. The operating points are defined by ambient temperature and humidity, passenger rate and solar radiation. In addition, the annual operating hours in each operating point are given for climate zones I to III. OPs with high ambient temperature, such as OP7, are considered to have more annual hours in standardized operation of climate zone I. In contrast, OPs with low ambient temperatures, such as OP8, are considered to have more annual hours in climate zone III. For the stated examples of OP7 and OP8, there are even different versions of the respective OP adjusted to different climate zones, for example, OP8_II for climate zone II and OP8_III for climate zone III. The operating hours add up to 7300 h out of 8760 h per year, which is equal to 20 h per day. A total of 4380 h are assigned to commercial operation in OP1-OP7, 1460 h to non-commercial operation in OP8-OP13, and 1460 h to parking operation in OP14–OP16.

In addition to environmental boundary conditions, three different track profiles are specified for this study. The specifications of the profiles are presented in Table 2. The tracks are chosen due to their non-electrified sections, so that they would be suitable for battery-electric rail vehicle operation. The track length is between 52 km and 87 km, which corresponds to a travel time between 57 min and 99 min.

Table 1. Standardized operating points over the year for regional rail vehicles according to EN 50591 [19].

OP	Ambient Temperature in °C	Ambient Relative Humidity in %	Passenger Rate in %	Solar Radiation in W/m²	Annual Hours Zone I	Annual Hours Zone II	Annual Hours Zone III
OP1	−10	90	0	0	2	65	372
OP2	0	90	100	0	244	945	1445
OP3	10	90	50	0	1086	1442	1198
OP4	15	90	50	0	1163	1102	889
OP5	22	80	100	0	969	627	404
OP6_I	28	70	100	600	695		
OP6_II	28	70	100	600		185	
OP6_III	28	50	100	600			72

OP7_I	40	40	100	800	221		
OP7_II	35	50	100	700		14	
OP8_II	−20	90	0	0		0	
OP8_III	−40	90	0	0			15
OP9	−10	90	0	0	0	21	109
OP10	0	90	0	0	175	490	638
OP11	15	80	0	0	657	674	539
OP12	22	80	0	0	533	257	143
OP13_I	40	40	0	800	95		
OP13_II	35	50	0	700		18	
OP13_III	28	70	0	600			16
OP14	0	90	0	0	175	512	762
OP15	15	80	0	0	827	801	629
OP16	28	50	0	700	458	147	69

Table 2. Specifications of track scenarios.

Track	Start/End Station	Length in km	Number of Stations	Travel Time in min
T1	Memmingen–Ulm	52.3	10	57.0
T2	Trier–Gerolstein	68.4	17	78.6
T3	Wangen–Sigmaringen	87.2	13	99.3

The vehicle velocity and catenary availability for the three different track scenarios are displayed in Figure 8. The velocity profiles show fast acceleration after every station, followed by a constant velocity close to the local speed limit before deceleration to the next station. The maximum velocity reached is 140 km/h. The catenary is available at sections where the catenary availability is 1. These sections are either at the beginning or the end of the track, as the catenary is mostly available at the main stations where the vehicles also start their operation. As soon as the catenary availability is 0, the electrical power supply for the rail vehicle is provided by the battery system.

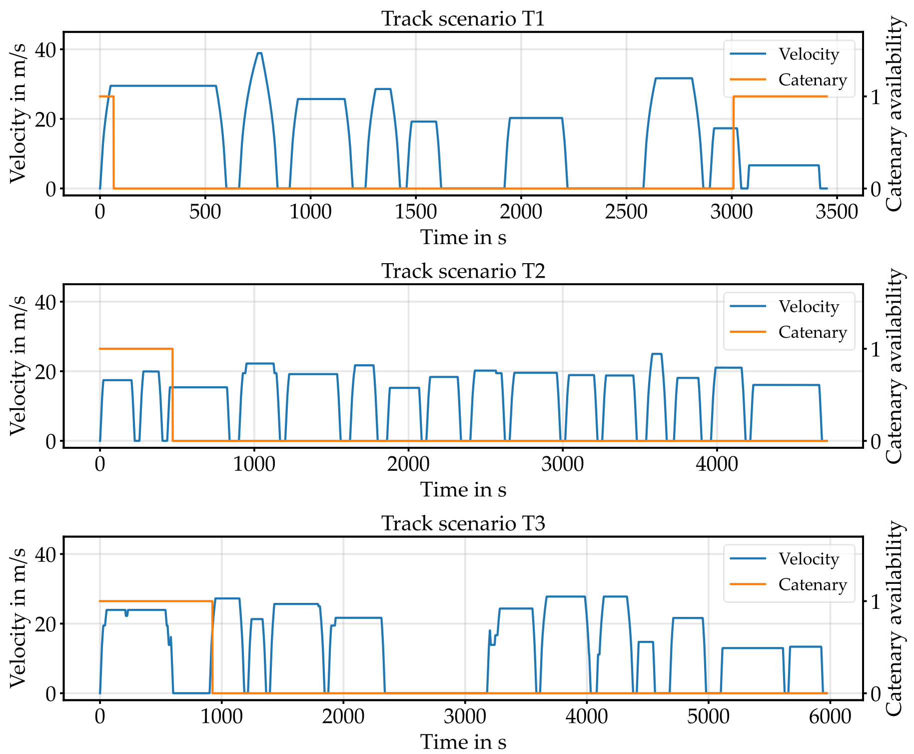

Figure 8. Vehicle velocity and catenary availability for reference tracks T1, T2 and T3.

https://doi.org/10.3390/en19173990

In addition to the track specifications, a generic BEMU is specified for this study. The specifications are summarized in Table 3. The specified reference vehicle is a two-car BEMU with a length of 45 m. Length, width, and height are important to determine the surface area for the thermal car body and the corresponding heat transfer. The maximum number of passengers is defined as 100. Thermal properties, including the thermal transmittance and heat transfer coefficients at walls and windows, have been defined based on EN 14750.

Table 3. Specifications and thermal properties of reference battery-electric rail vehicle.

Specification	Unit	Value
Number of cars	-	2
Length	m	45.0
Width	m	2.8
Height	m	3.4
Thermal transmittance wall	W/m^2K	2.23
Thermal transmittance window	W/m^2K	5.6
Heat transfer coefficient wall inside	W/m^2K	10
Heat transfer coefficient window inside	W/m^2K	10
Max. passengers	-	100
Battery energy content	kWh	500

The operation of the HVAC system in this study is based on the parameters given in EN 14750. Set points for fresh air volume flow and temperature in the cabin, depending on ambient temperature, are summarized in Figure 9. A minimum and maximum cabin temperature set point is defined in EN 14750, depending on ambient temperature. Additionally, a recommended set-point curve is given, which has values between minimum and maximum. As part of this study, two optimized set-point curves were developed for operation with and without catenary, as presented in Figure 9 on the right. The corresponding thermal management strategy is introduced in Figure 5. For very high and very low temperatures, the curves define lower temperature differences to the ambient temperature and lower fresh air volume flows to reduce energy demand. The fresh air volume flow is defined per passenger in the vehicle. A minimum fresh air volume flow of 400 m^3/h is assumed, even if the passenger number is very low. This assumption is based on EN 14750, which recommends a minimal fresh air volume flow of 4 m^3/h times the maximum number of passengers.

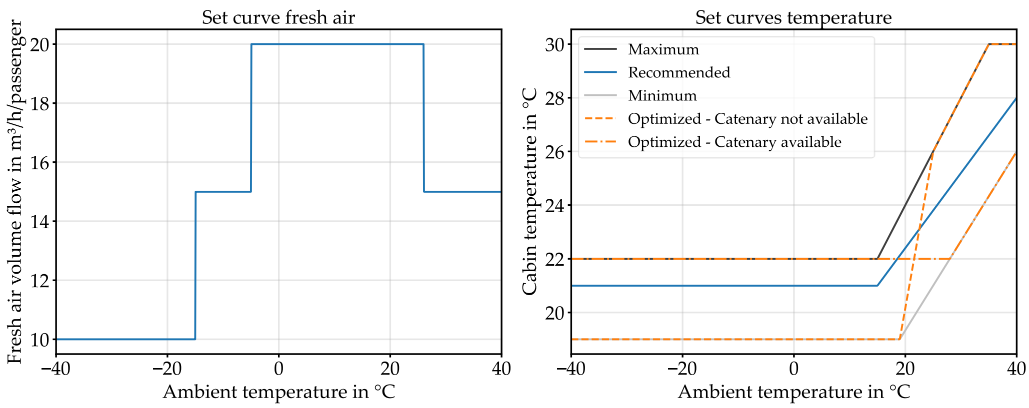

Figure 9. Set-point curves for fresh air volume flow and cabin temperature, depending on ambient temperature.

3. Results—Simulated Energy Demand in Battery-Electric Rail Vehicles for Different Climate Zones

The following section presents how the energy demand in battery-electric rail vehicles is affected by heat pump application with different refrigerants. It shows how efficiency varies over operating points and operation in different climate zones. Additionally, the effects of the optimized operating strategy on the cycling of the battery system are presented.

3.1. Energy Demand with Heat Pumps and Different Refrigerants

The energy demand for HVAC systems with heat pumps is calculated with the TCBM and heat pump model presented in Sections 2.1 and 2.2. The applied input parameter sets for these simulations are described in Section 2.4. The simulated energy demand for the reference vehicle on track T1 is displayed in Figure 10, based on the recommended set-point cabin temperature from Figure 9. It is presented for three different refrigerants, R744, R290, and R134a, and for the different operating points from Table 1. As some operating points, such as OP1 and OP9, have the same conditions, they are not presented separately.

OP8_III shows the highest thermal energy demand over all studied OPs, with 75 kWh in the 1 h track scenario T1. For cooling conditions, OP7_I shows the highest thermal energy demand with 55 kWh. In both cases, this results in the highest electrical energy demand using R744 as a refrigerant. In comparison, the results with R290 and R134a show a reduced energy demand because of higher COP values. In the most demanding heating conditions of OP8_III, the results for R744 show a higher electrical than thermal energy demand. As a result, resistance heaters would be more efficient than R744 heat pumps in these conditions. Nevertheless, the most demanding operating points do not occur often throughout the year, according to Table 1. In more moderate conditions, such as OP2, all refrigerants show a lower electrical than thermal energy demand. Consequently, the application of heat pumps increases the system efficiency compared to resistance heaters in these OPs, which occur often throughout the year, according to Table 1.

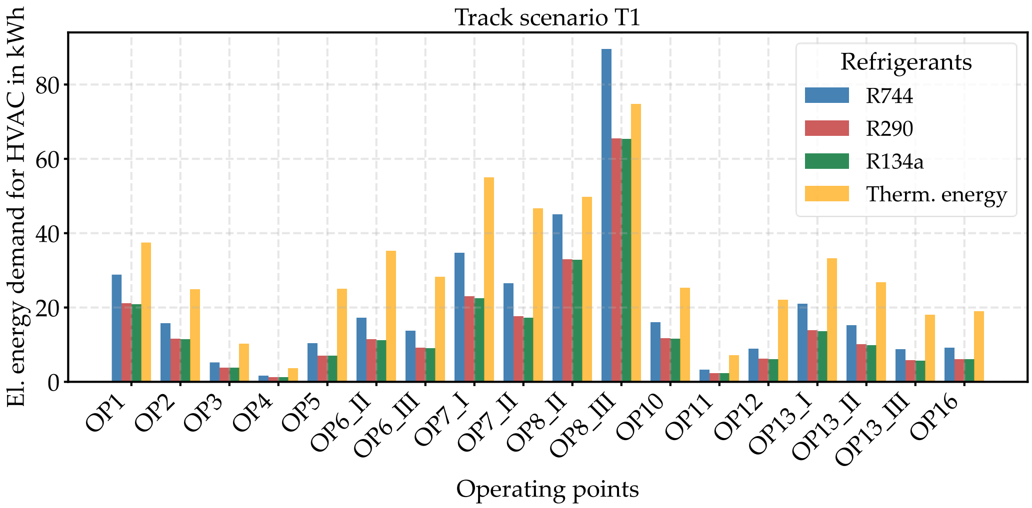

Figure 10. Track-specific electrical energy demand for HVAC in battery-electric rail vehicle for operating points from Table 1 and different refrigerants with recommended set-point cabin temperature in use case T1.

In addition to the route-specific energy demand, the annual energy demand for HVAC systems is calculated and presented in Figure 11. To calculate the annual demand, the average HVAC power demand over track T1 is multiplied by the annual hours for every OP from Table 1. The annual thermal energy demand can be calculated by adding the thermal demand for cooling and heating presented in Figure 11. For climate zone II, the annual demand for heating is 90 MWh and 20 MWh for cooling, resulting in an overall annual demand of 110 MWh. In comparison, energy demand is higher in climate zone I, with 131 MWh, and in climate zone III, with 138 MWh. It also shows that the thermal energy demand for heating is highest in climate zone III, with 123 MWh, which is equivalent to 89% of the thermal energy demand for HVAC in this zone. Only 11% is demanded for cooling. In contrast, the thermal energy demand for cooling is highest in climate zone I, with 75 MWh, which corresponds to 57% of total energy demand. Overall, the comparison between the different climate zones demonstrates that the thermal energy demand for heating is dominant compared to the one for cooling.

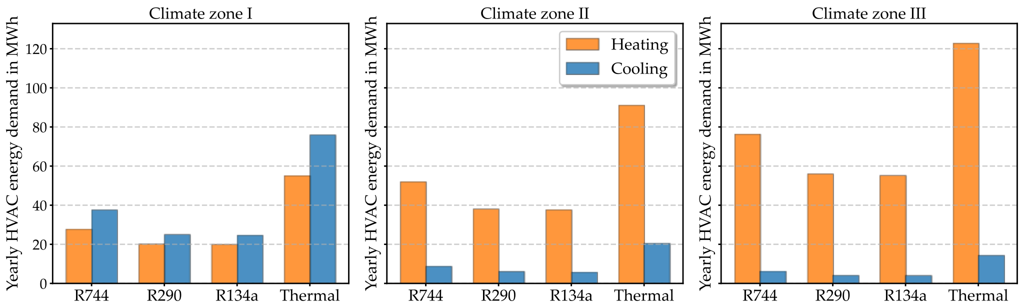

Figure 11. Annual electrical and thermal energy demand for heating and cooling of HVAC in battery-electric rail vehicle for climate zones I, II, III for different refrigerants based on power demand in use case T1.

Next to the thermal energy demand in Figure 11, the corresponding electrical energy demand for the different refrigerants is presented. The comparison shows that the R744 HVAC system requires the highest overall electrical energy demand, with 83 MWh in climate zone III combined for cooling and heating. R134a shows the lowest energy demand in climate zone II, with 43 MWh, whereas energy demand with R290 is only slightly higher at 44 MWh. In these cases, the same refrigerant is used for heating with a heat pump and cooling with air-conditioning mode. In state-of-the-art vehicles, heating is often performed with resistance heaters and cooling with vapor compression cycles with synthetic refrigerants, as stated in Section 1.3. To identify the respective values in Figure 11, the thermal energy demand for heating and the electrical energy demand for cooling with R134a need to be summed up, which results in 80 MWh in climate zone I, 97 MWh in zone II, and 127 MWh in zone III. Compared with these state-of-the-art values, heat pump operation with natural refrigerants R744 and R290 reduces the energy demand for the HVAC system in all climate zones. The highest reduction in energy demand occurs in climate zone II because of the moderate operating conditions. The heat pump application for R744 reduces annual energy demand compared to the state-of-the-art HVAC systems by 37% to 36.1 MWh, and the application for R290 by 55% to 53 MWh.

Overall, the results show that heat pumps with certain natural refrigerants can lead to a higher energy demand on single routes at very low temperatures. However, they are able to reduce energy demand for battery-electric rail vehicles significantly in moderate conditions and especially over a full year of operation throughout all four seasons.

3.2. Optimized Thermal Management Strategy for HVAC Operation

The previous section demonstrates how the HVAC energy demand for battery-electric rail vehicles can be reduced to increase range in operation by using natural refrigerants. Even higher ranges are possible if the operating strategy of the HVAC system is adjusted. An optimized operating strategy based on set-point temperatures, which depend on catenary availability, was introduced at the end of Section 2.2 and in Figure 9. The effect of this optimized thermal management strategy is displayed in Figure 12.

As the presented operating point OP1 is a heating case, the set-point temperature in sections without catenary availability is reduced for these track sections. The first change in catenary availability occurs after around 60 s, which leads to a decrease in the set-point temperature from 22 °C to 19 °C. Accordingly, the actual cabin temperature follows this new set-point value. At around 3000 s, the catenary availability returns, and the set-point temperature increases again to 22 °C. On the right side of Figure 12, the corresponding power demand of the HVAC system is presented. The reference operating strategy, which follows the recommended set-point temperature and does not change with catenary availability, shows an HVAC power demand of around 39 kW, with small fluctuations caused by the change in vehicle velocity. In contrast, the optimized strategy reduces power demand from 41 kW to 24 kW after the change in catenary availability at 60 s. Afterwards, the power demand increases up to around 36 kW. This demand does not occur immediately after the change because the cabin is still charged thermally due to the higher set-point temperature in the section before. This leads to a lower power demand after the change in catenary availability, compared to a more stationary operation in sections without catenary. At the second change in catenary availability after 3000 s, the power demand increases from 36 kW to 53 kW. After this change, a reverse effect can be seen. Directly after the catenary is available, again the power demand peaks as the cabin needs to be re-heated by the 3 K temperature difference between the set-point temperatures of 19 °C and 22 °C. After the re-heating process is completed, the power demand reaches the initial value of around 42 kW again.

The integration of the power demand curves from Figure 12 shows that the reference strategy has an energy demand of 5.5 kWh in sections with catenary and 31.9 kWh in sections without catenary. In contrast, the optimized strategy shows an energy demand of 6.3 kWh in sections with catenary and 28.9 kWh without catenary. Thus, energy demand is increased in sections with catenary by 14% but was reduced in sections without catenary by 10%. The energy demand is also reduced over the whole T1 track compared to the reference set-point curve, although this depends heavily on the length of the section without catenary. Longer sections with catenary available could lead to an increase in energy demand with the optimized set-point curve. Overall, the presented optimized thermal management leads to an increase in energy demand within sections where electrical energy is available through catenary, and to a decrease in energy demand within sections where the electrical energy needs to be provided by the battery system. This leads to a reduced load on the battery and an additional range for the vehicles in operation.

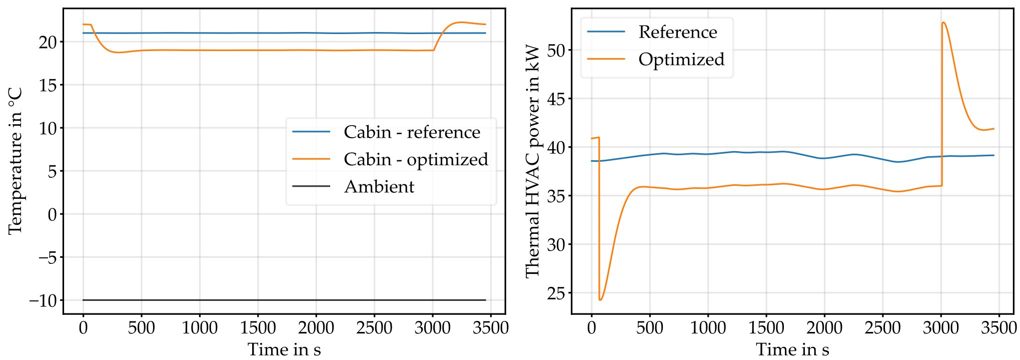

Figure 12. Simulated temperature in the cabin (**left**) and thermal energy demand (**right**) for track T1 in OP1 with and without optimized thermal management strategy.

3.3. Advantages for the Cycling of the Battery System

The reduced energy demand on the battery system with an optimized thermal management strategy is presented in the previous sections. This section focuses on the effects and advantages which occur due to the reduced energy demand for the battery system. The energy content for the battery system studied in the following is 500 kWh, as presented in Table 3. The studied refrigerant for this section is R290. Figure 13 presents how the SoC of the battery system in the vehicle develops in use cases T1, T2, and T3. The curves are calculated based on traction, HVAC, and auxiliary power profiles in the vehicle, respecting common efficiencies of the power components.

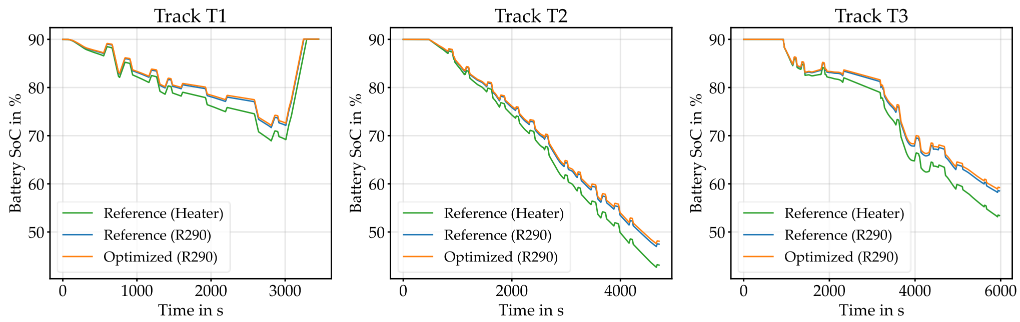

Figure 13. Battery system SoC over time for T1, T2 and T3 in OP1 with and without optimized operating strategy.

The SoC curves show different characteristics between the studied tracks. For T1, it can be seen that the SoC increases near the end at 3000 s as the vehicle arrives in a section with catenary and uses this electrical power supply to recharge the battery. For the other two tracks, no recharging occurs in the operation, as no catenary is available at the final station. In contrast, in T2 and T3, the SoC is kept constant at the beginning of the track until the catenary is no longer available after around 500 s and 1000 s, respectively. In T2, the lowest SoC is 43%, as this track has the highest number of stations and therefore acceleration and deceleration processes without trackside electrification. In all track scenarios, the optimized thermal management strategy results in higher SoC values compared to the reference strategy. For the presented tracks in Figure 13, the SoC is up to 1% higher in the optimized R290 strategy at the end of T2 compared with the reference strategy with R290. Compared to the reference strategy with resistance heaters, the SoC for the optimized R290 strategy is up to 5% higher. On the vehicle level, the reduced energy demand leads to an increase in available range. The reference R290 scenario increases the range by 9% compared to the reference heater scenario. If the optimized thermal management strategy is applied, the range can be increased further by another 1% at this operating point. For OP8_III, the range increase from the R290 reference case to the R290 optimized case is 2%. As the range increase depends on HVAC energy demand, it is higher for operating points with higher HVAC energy demand.

In addition to an increased range and SoC, the battery system is also cycled less with the optimized strategy. The cycling of the battery is measured in equivalent full cycles (EFCs), which show how often the overall battery capacity is discharged and charged by partial cycles in operation. Charging takes place in sections with catenary or by regenerative braking. Figure 14 shows how many EFCs are simulated for the reference and optimized operating strategy at the different tracks. EFC values are around 0.3 cycles for T1 and around 0.32 cycles for T2. In T2, the battery is discharged to lower SoC values because there are more stations than in T1, but in T1, it is recharged to the initial SoC at the end of the track. Recharging in scenario T2 would increase the EFCs in this cycle by around 0.25.

At track T3, the number of cycles is around 0.29 and therefore lower compared with T1 and T2, as the number of stations is lower and no recharging is performed. For all tracks, the EFCs are reduced with the optimized strategy compared to the reference. The reduction with the optimized strategy is 0.004 EFC for T1, which means a relative reduction in EFC of 1.4%. With 12 trips per day, this results in a reduction of around 18 EFC per year.

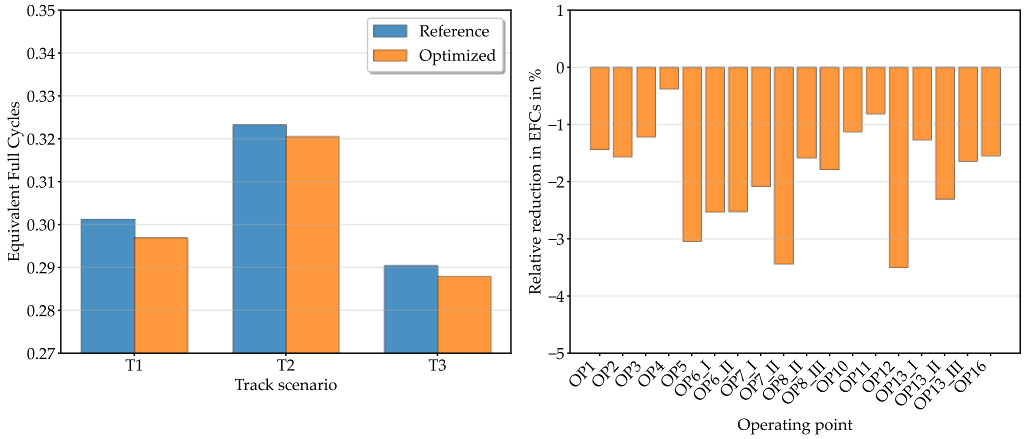

Figure 14. Equivalent full cycles of the battery with and without optimized thermal management strategy for T1, T2, T3 in OP1 (**left**) and relative reduction in equivalent full cycles with optimized thermal management strategy for different operating points for T1 (**right**).

The effect of the optimized strategy on the EFC depends on the operating conditions of the vehicle, as presented in Figure 14 on the right. The relative reduction in EFCs is given for the different operating points in Table 1 and shows values between 0.9% and 3.5%. The minimal relative reduction occurs at OP4 and OP11, as the HVAC energy demand in these OPs is very low, as presented in Figure 10. The maximum reduction in relative EFCs occurs at OP7_II, which is a cooling case. In general, the OPs where cooling is required show a higher reduction in relative EFCs, as less energy for dehumidification is also necessary. For heating cases, the maximum reduction in relative EFCs appears in OP8_II with 1.8%. Overall, it becomes clear that optimized operation of the HVAC system in a battery-electric vehicle reduces energy demand from the battery system and provides a higher lifetime of the battery system in the vehicle.

4. Discussion

Models for the thermal car body and HVAC system with a heat pump are developed and simulated in the presented paper to study the effects of heat pumps and efficient thermal management strategies on the operation of battery-electric rail vehicles. Results for efficient thermal management strategies are specific to battery-electric rail vehicles, whereas the study of energy efficiency of heat pumps with different refrigerants can also be applied to other kinds of rail vehicles.

The results show that energy demand for HVAC systems in battery-electric rail vehicles is similar for the natural refrigerant R290 and the synthetic refrigerant R134a. R744, as an alternative natural refrigerant, shows a lower energy efficiency in the calculated COP curves based on the vapor compression cycle, resulting in a higher HVAC energy demand. At operating points with very low ambient temperatures, COP values are similar to 1 or even below, depending on the refrigerant. This means that heat pump operation is not providing a significantly higher efficiency than resistance heaters under these conditions. In more moderate operating points with less extreme ambient temperatures, heat pump operation with all three studied refrigerants is more efficient than heating with resistance heaters. These moderate conditions occur more frequently throughout the year, which leads to a reduction in the annual HVAC energy demand by over 50% when heat pumps are utilized. Furthermore, this enables an increased range for the vehicles in operation and a reduced load on the battery system.

In addition, the load on the battery can be reduced with an optimized thermal management strategy. The strategy includes the dynamic change in set-point temperatures in the cabin based on the availability of electrical power supply from the catenary. For heating cases, it reduces the load on the battery by reducing overall HVAC energy demand. For cooling cases, this strategy leads to even further reductions in the cycles at the battery because it also reduces energy demand for dehumidification. Especially at high and very low ambient temperatures, the strategy achieves a high relative reduction in equivalent full cycles at the battery system. Overall, the strategy represents a feature for battery-electric rail vehicles that does not require the installation of additional components but increases lifetime of the battery system and additional range at very demanding operating conditions.

Battery-electric rail vehicles are required to have low impact on the environment and provide high range and flexibility in daily operation in all kinds of operating conditions. State-of-the-art rail vehicles are often equipped with synthetic refrigerants for cooling and resistance heaters for heating. Natural refrigerants like R290 or R744 are suitable options for heating with heat pumps, providing a lower environmental impact and high energy efficiency, especially with R290.

Current thermal management strategies in rail vehicles define set-point temperatures based on ambient temperature. The developed optimized operating strategy also takes into account the catenary availability for battery-electric rail vehicles. Such a thermal management strategy could be implemented in current vehicles, as no additional components are required, and only control mechanisms need to be adjusted. New heat pump systems with natural refrigerants could also be implemented in current vehicles. However, this would require high effort in system integration or a complete replacement of the current HVAC modules. Since this is a very cost-intensive process, heat pumps with natural refrigerants are suitable for newly manufactured rail vehicles in particular. The state-of-the-art battery systems used in rail vehicles, LTO batteries, benefit highly from the reduced load and cycling in the system. A relative reduction in equivalent full cycles leads to a higher increase in absolute lifetime, as the overall lifetime cycles are higher than with other battery chemistries like LFP.

The studied results are based on simulations performed with the developed thermal car body and heat pump model. For the modeling, different assumptions lead to limitations in the evaluation of the results. The heat pump model generating the COP curves is based on the vapor compression cycle and an empirical factor describing the difference between the ideal COP in the vapor compression cycle and the real COP measured in rail vehicles. The results are sensitive to the parametrization of this factor, which is why the chosen factor and the calculated COP curves are validated by comparison with references from the literature. The transcritical modeling of R744 is based on the extrapolation from subcritical operating points. This represents a simplification that only affects a small number of operating points in this study, as most of them use subcritical conditions to evaluate energy demand. Nevertheless, for future detailed analysis of these transcritical operating points, an individual validation of the simplified transcritical modeling approach needs to be performed. A physical modeling of all sub-components in the HVAC system with a heat pump is not performed. This limits the analysis to the energy efficiency based on the modeled COP curves, not taking into account the available thermal heating power based on limited compressor power. For R744 as a refrigerant, this can provide additional advantages at low ambient temperatures, as the heating power is higher than with R290 and

R134a, if compressors are designed for refrigeration. The thermal car body model is based on the heat transfer through the walls and the pre-conditioning of the air for the cabin. A lumped parameter approach is chosen, which can be extended in future work by developing and implementing a multi-zone model of the cabin to take into account temperature distribution. Air exchange through sealings or door openings is currently not simulated specifically in the thermal car body model. This air exchange can be seen as part of the exhaust air already simulated in the model, but a specific modeling of these processes would increase the level of detail in the model. As the modeled vehicles are operating as regional rail vehicles between cities, door openings are not frequently in operation. If the scope of the study were increased to inner-city operation of rail vehicles like metro vehicles, door openings and the corresponding air exchange would become more relevant in their effect on energy demand. Nevertheless, model validation shows that results for the overall energy demand in simulation and measurement are comparable to each other. It needs to be mentioned that the interpretation of the measurement data has some limitations as well. For example, radiation, air exchange due to leakage, and door opening are not measured in the vehicles and need to be assumed in the models. Also, cabin temperature fluctuates in daily operation because of transient effects like passengers leaving and entering the vehicle. For the simulations with the validation parameter sets, more constant cabin temperatures occur because of fewer transient effects. In the parameter sets for the evaluation of heat pumps and thermal management strategies, standardized constant operation points from EN 50591 are defined. Transient effects like changes in passenger rate and temperature increases or decreases in the cabin are not part of these operating points. Effects of rapidly changing weather and timetable delays can occur in real vehicle operation but are not included in the standardized evaluation of vehicle energy demand based on EN 50591 and therefore not considered in this study. The climate zones evaluated are limited to climate conditions in Europe. Globally, other climate conditions like tropical climates exist but are more focused on cooling instead of heating and are therefore less relevant for the evaluation of heat pumps. The standardized year of operation used for the calculation of annual energy demand is not representative of all possible locations for the operation of battery-electric rail vehicles. Special local conditions could lead to different results in annual energy demand, especially if more extreme operating conditions occur more often than in the standardized year. This could be the case in continental climates that occur, for example, in Eastern Europe. The study is also limited to three highly discussed refrigerants for rail vehicles. Many more refrigerants are available and discussed in other applications such as passenger cars, buses, or stationary HVAC systems.

In future work, the methodical approach of this study can be extended to other new refrigerants with low environmental impact, synthetic, and natural ones to investigate their effect on the operation of battery-electric rail vehicles. In addition, more parameter sets of different vehicles can be studied to assess the effect of vehicle size on HVAC energy demand. Furthermore, demonstrators of heat pump systems with different refrigerants can be built to measure and validate the studied effects on the hardware components. The measurement results can also be used to develop and validate individual models of the different sub-components in the heat pump system. When developing demonstrators, the design process for heat pumps in battery-electric rail vehicles should be focused on. Currently, vapor compression cycles in HVAC systems are mainly designed for cooling operation, and heat pump operation is added by reversing these cycles. A design of the vapor compression cycle, especially for heat pump operation, can lead to a different setup with different effects concerning energy demand in daily operation. For a comprehensive analysis of these HVAC systems, the amount of refrigerant, leakage safety, high-pressure operation and fan losses should be studied for future setups of the systems. In addition to the heat pump system, the optimized thermal management strategy can be demonstrated

https://doi.org/10.3390/en19173990

in vehicles in future work. This offers the opportunity to validate the calculated relative reduction in equivalent full cycles with vehicles in operation. The calculated and measured equivalent full cycles can also be used in future work to study the behavior of battery aging in rail vehicles. For the continuous operation of battery-electric rail vehicles, this aging behavior is highly relevant because of its effect on maintenance cost. By demonstrating the thermal management strategy, the thermal comfort of passengers in the vehicles can also be evaluated to identify whether changes in set-point cabin temperature lead to a change in comfort perceived by passengers. For a further extension of this study in future work, the operating costs of heat pumps in battery-electric vehicles can be analyzed and combined with an overall investigation of lifecycle cost and assessment. This would enable a more detailed evaluation of heat pump technology in a rail-specific context concerning cost and impacts on climate and the environment. The presented analysis of energy demand and efficiency is one important aspect and serves as a base for these further investigations.

More battery-electric rail vehicles will likely be procured and operated in the future to replace rail vehicles operating with diesel. Heat pumps with natural refrigerants like R290 increase energy efficiency and therefore range in these vehicles and enable operation with low environmental impacts. In very demanding operating conditions with high and low temperatures, an optimized thermal management strategy helps to maintain this range for the vehicles if the set-point temperature in the cabin is adjusted to catenary availability. Consequently, battery-electric rail vehicles offer more flexibility and availability in daily operations, leading to higher acceptance among rail vehicle operators adapting to this new sustainable mobility.

5. Conclusions

Battery-electric rail vehicles are used as an alternative to diesel rail vehicles for track sections without electrical power supply via catenary. However, the battery capacity limits the range of the vehicles, and the applied refrigerants in their HVAC systems are harmful to the environment. This is why the presented work studies heat pumps with natural refrigerants, optimized thermal management strategies and their resulting energy demand on the battery system in the operation of battery-electric rail vehicles.

A thermal car body model and heat pump model are developed and validated to calculate the electrical energy demand of battery-electric rail operation. As parameter sets, three different climate zones, operating points defined in EN 50591, three different tracks, and a generic BEMU with a battery energy content of 500 kWh are studied. Thermal comfort in the vehicle is defined based on EN 14750 values for set-point cabin temperature.

The simulation results show that thermal energy demand for HVAC systems is up to 75 kWh for a one-hour track scenario. The results are specific to regional passenger rail vehicles, as battery-electric passenger cars have a different cabin shape and size, and different standards for thermal comfort. The electrical energy demand for HVAC systems that are using heat pumps with R290 as a natural refrigerant is similar to a system with the synthetic refrigerant R134a. In comparison, heat pump systems with the natural refrigerant R744 are less efficient and show a higher electrical energy demand, based on the simulated COP values. Nevertheless, under moderate operating conditions, such as 0 °C, heat pump operation with all three studied refrigerants shows a significantly higher coefficient of performance than state-of-the-art resistance heaters. In contrast, for very low temperatures such as −40 °C, the electrical HVAC energy demand with resistance heaters is similar to heat pump systems. Compared over a standardized year of operation, these extreme temperatures do not occur as frequently as moderate conditions, and the electrical energy demand of HVAC systems with heat pumps is significantly lower than with resistance heaters. This applies to all three studied climate zones, even though the highest relative reduction in energy demand occurs in climate zone II, which makes it especially suitable for heat pump application. The simulated annual thermal energy demand in climate zone II, which represents Central Europe, is 110 MWh for a generic two-car BEMU. The annual electrical energy demand is reduced by 55% based on the modeled COP curves for an R290 HVAC system compared to a state-of-the-art HVAC system with a resistance heater and R134a for refrigeration.

Optimized thermal management strategies can reduce this energy demand at the battery even further. Battery-electric rail vehicles operate partly in sections with and without catenary. An optimized thermal management strategy is developed, which dynamically adjusts the set-point temperature in the cabin depending on catenary availability. With this strategy, HVAC power demand increases in sections with catenary and decreases in sections without. As a consequence, the battery is cycled less. Equivalent full cycles are reduced by up to 3% in a 1 h track scenario with 0.3 equivalent full cycles. The optimized strategy is especially suitable for operating points with high HVAC energy demand at low or high temperatures and therefore vehicle operation in climate zones I and III.

Overall, rail-vehicle thermal management is strongly affected by refrigerant characteristics, passenger load, weather conditions, catenary availability, route profiles, and battery states. Integrating dynamic thermal management strategies with adaptive and route-specific control can further reduce battery loads while maintaining passenger comfort. Energy demand and battery load can be reduced by heat pumps with natural refrigerants and optimized thermal management strategies in battery-electric rail vehicles. Enhanced range, vehicle availability, and flexibility in daily operation demonstrate that HVAC and thermal management systems are critical to increasing operator acceptance of battery-electric rail vehicles. Therefore, this leads to more sustainable public rail transport.

Author Contributions: S.W.: Writing—original draft, visualization, validation, supervision, software, methodology, investigation, formal analysis, conceptualization. M.S.: Writing—review and editing, software, methodology. L.B. (Linus Brünner): Writing—review and editing, software, methodology. L.B. (Lutz Boeck): Writing—review and editing. All authors have read and agreed to the published version of the manuscript.

Funding: This research received no external funding.

Data Availability Statement: The data presented in this study is not publicly available due to its size and complexity but is available on request from the corresponding author.

Acknowledgments: The authors acknowledge Hunter Adams and Dylan Finlay from the German Aerospace Center for supporting the simulation process.

Conflicts of Interest: Author Lutz Boeck was employed by the company Wabtec Germany GmbH. The remaining authors declare that the research was conducted in the absence of any commercial or financial relationships that could be construed as a potential conflict of interest.

Nomenclature

The following abbreviations and symbols are used in this manuscript:

AC	Alternating Current
BEMU	Battery-Electric Multiple Unit
COP	Coefficient of Performance
DC	Direct Current
DLR	German Aerospace Center
EER	Energy Efficiency Ratio
EFC	Equivalent Full Cycle
El.	Electrical

EN	European Norm
EU	European Union
GWP	Global Warming Potential
HVAC	Heating, Ventilation, Air Conditioning
LFP	Lithium Iron Phosphate
LTO	Lithium Titanium Oxide
MDPI	Multidisciplinary Digital Publishing Institute
NMC	Lithium Nickel Manganese Cobalt Oxide
OESS	On-board Energy Storage System
OP	Operating Point
PFAS	Polyfluoroalkyl Substances
R1234yf	Refrigerant: 2,3,3,3-Tetrafluoropropene
R134a	Refrigerant: 1,1,1,2-Tetrafluorethane
R290	Refrigerant: Propane
R407C	Refrigerant: Mixture of R32 (23%), R125 (25%), and R134a (52%)
R410A	Refrigerant: Mixture of R32 (50%), R125 (50%)
R729	Refrigerant: Air
R744	Refrigerant: CO_2
SoC	State of Charge
TCBM	Thermal Car Body Model
TFA	Trifluoroacetic Acid
Therm.	Thermal
TRL	Technology Readiness Level
α_i	Heat transfer coefficient for convection inside
α_o	Heat transfer coefficient for convection outside
$\alpha_{o,wall}$	Heat transfer coefficient for convection at outer wall
$\alpha_{o,window}$	Heat transfer coefficient for convection at outer window
λ	Thermal conductivity
A	Area
C	Heat capacity
COP_{ideal}	COP in ideal vapor compression cycle
$COP_{ideal,cool}$	COP in ideal vapor compression cycle
$COP_{ideal,heat}$	COP in ideal vapor compression cycle
COP_{real}	COP in real vapor compression cycle
d	Thickness
f_{COP}	Factor for ratio between ideal and real COP
Δh_{cb}	Change in specific enthalpy of the air in the cabin over a time step
h_1	Specific enthalpy after evaporator in vapor compression cycle
h_2	Specific enthalpy after compressor in vapor compression cycle
h_3	Specific enthalpy after condenser in vapor compression cycle
h_4	Specific enthalpy after expansion valve in vapor compression cycle
$h_{cb,t}$	Specific enthalpy of the air in the cabin at time step t
$h_{cb,t+1}$	Specific enthalpy of the air in the cabin at time step t + 1
h_{in}	Specific enthalpy of the air entering the cabin
h_{out}	Specific enthalpy of the air leaving the cabin
h_{Pass}	Specific enthalpy of vaporization of water emitted from passengers
h_v	Vaporization enthalpy of water
H	Absolute enthalpy
m_{cb}	Mass of air in the cabin
$m_{w,cb}$	Mass of water in the cabin
$\dot{m}_{in}$	Mass flow of air entering the cabin
$\dot{m}_{Pass}$	Mass flow of water emitted by the passengers
$\dot{m}_{out}$	Mass flow of air leaving the cabin
$p_{sat,Tcond}$	Saturation pressure at condenser temperature
$p_{sat,Tevap}$	Saturation pressure at evaporator temperature
P_{El}	Electrical power
Q_{cond}	Heat exchanged at condenser
Q_{evap}	Heat exchanged at evaporator
$\dot{Q}_{Cond,i}$	Heat flow from conduction at inside

https://doi.org/10.3390/en19173990

$\dot{Q}_{Cond,o}$	Heat flow from conduction at outside
$\dot{Q}_{Conv,i}$	Heat flow from convection at inside
$\dot{Q}_{Conv,o}$	Heat flow from convection at outside
$\dot{Q}_{Cool,therm}$	Heat flow to cool mixed air
$\dot{Q}_{El}$	Heat flow from electrical heating
$\dot{Q}_{Heat,therm}$	Heat flow to heat mixed air
$\dot{Q}_{Pass}$	Heat flow from passengers
$\dot{Q}_{Pass,lat}$	Latent heat flow from passengers
$\dot{Q}_{Rad}$	Heat flow from radiation
$\dot{Q}_{Rad,abs}$	Heat flow from radiation absorbed by the wall
$\dot{Q}_{Rad,emit}$	Heat flow from radiation emitted by the wall
$\dot{Q}_{Trp}$	Heat flow through heat transport
s_1	Specific entropy after evaporator in vapor compression cycle
s_2	Specific entropy after compressor in vapor compression cycle
t	Time
Δt	Change in time / time step
T	Temperature
T_{amb}	Ambient temperature
T_{cb}	Temperature in cabin
T_{cond}	Temperature at condenser
T_{evap}	Temperature at evaporator
$T_{Surf,i}$	Surface temperature inside
$T_{Surf,o}$	Surface temperature outside
T_t	Temperature at time step t
T_{t+1}	Temperature at time step t+1
v	Velocity
$\dot{V}_{CA}$	Volume flow of circulating air
$\dot{V}_{CEA}$	Volume flow of cabin entering air
$\dot{V}_{EA}$	Volume flow of exhaust air
$\dot{V}_{FA}$	Volume flow of fresh air
$\dot{V}_{MA}$	Volume flow of mixed air of recirculating air and fresh air
W_{comp}	Work of compressor
Δx_{cb}	Change in absolute humidity over a time step
$x_{cb,t+1}$	Absolute humidity in the cabin at time step t+1
x_{in}	Absolute humidity of the air entering the cabin
x_{out}	Absolute humidity of the air leaving the cabin

References

1. Eurostat. *Length of Railway Lines by Number of Tracks and Electrification of Lines*; Eurostat: Luxembourg, 2026. https://doi.org/10.2908/RAIL_IF_LINE_TR.
2. Chamaret, A.; Mannevy, P.; Clément, P.; Ernst, J.; Flerlage, H. Analysis, trends and expectations for low carbon railway". *Transp. Res. Procedia* **2023**, *72*, 2684–2691. https://doi.org/10.1016/j.trpro.2023.11.808.
3. Wieser, S.; Brünner, L.; Böhm, M.; Soto, M.; Rodríguez, E.J. Development, application and optimization of hydrogen refueling processes for railway vehicles. *Int. J. Hydrogen Energy* **2025**, *124*, 331–344. https://doi.org/10.1016/j.ijhydene.2025.04.040.
4. Streuling, C.; Pagenkopf, J.; Schenker, M.; Lakeit, K. Techno-Economic Assessment of Battery Electric Trains and Recharging Infrastructure Alternatives Integrating Adjacent Renewable Energy Sources. *Sustainability* **2021**, *13*, 8234. https://doi.org/10.3390/su13158234.
5. Schenker, M.; Schirmer, T.; Dittus, H. Application and improvement of a direct method optimization approach for battery electric railway vehicle operation. *Proc. Inst. Mech. Eng. Part F J. Rail Rapid Transit* **2021**, *235*, 854–865. https://doi.org/10.1177/0954409720970002.
6. Wieser, S.; Schenker, M.; Schwurack, H.; Hoffmann, F.; Donner, S.; Konrad, M. Efficient Air Conditioning of Battery-Electric Multiple Units (BEMU): Modeling and Optimization. In *Transport Transitions: Advancing Sustainable and Inclusive Mobility*. McNally, C., Carroll, P., Martinez-Pastor, B., Ghosh, B., Efthymiou, M., Valantasis-Kanellos, N., Eds.; Springer Nature Switzerland: Cham, Switzerland, 2025; pp. 485–491. https://doi.org/10.1007/978-3-031-89444-2_71.

7. Boev, P.; Zimmermann, U.; Ebrecht, B.; Mach, S. von. First Passenger Operation of a State-of-the-art Battery-Electric Multiple Unit (BEMU) in Germany. *Transp. Res. Procedia* **2023**, *72*, 2510–2517. https://doi.org/10.1016/j.trpro.2023.11.757.
8. Bitterberg, U. XMU-Triebzüge für den SPNV in Deutschland Stand der Markteinführung Frühjahr 2025 (engl. XMU multiple units for regional rail transport in Germany Market launch scheduled for spring 2025). *ETR Eisenbahntechnische Rundsch.* **2025.**
9. Juston, M.; Chamaret, A.; Renault, M.; Vulturescu, B. Ecosystem Analysis of the Battery Train, Today and in the Future. In *Transport Transitions: Advancing Sustainable and Inclusive Mobility*; McNally, C., Carroll, P., Martinez-Pastor, B., Ghosh, B., Efthymiou, M., Valantasis-Kanellos, N., Eds.; Springer Nature Switzerland: Cham, Switzerland, 2025; pp. 552–557. https://doi.org/10.1007/978-3-031-89444-2_81.
10. Kapetanović, M.; Núñez, A.; van Oort, N.; Goverde, R.M. Energy use and greenhouse gas emissions of traction alternatives for regional railways. *Energy Convers. Manag.* **2024**, *303*, 118202. https://doi.org/10.1016/j.enconman.2024.118202.
11. Fedele, E.; Iannuzzi, D.; Del Pizzo, A. Onboard energy storage in rail transport: Review of real applications and techno-economic assessments. *IET Electr. Syst. Trans.* **2021**, *11*, 279–309. https://doi.org/10.1049/els2.12026.
12. Herwartz-Polster, S.; Böhm, M.; Stickel, S.; Streuling, C.; Hertel, B.; Pagenkopf, J. Applications—Transportation Applications | Rail Vehicles—Fuel Cells and Batteries. In *Encyclopedia of Electrochemical Power Sources*; Elsevier: Amsterdam, The Netherlands, 2025; pp. 268–279. https://doi.org/10.1016/B978-0-323-96022-9.00051-7.
13. Raeesi, M.; Laleh, A.A.; Shojaeefard, M.H.; Chavoshnia, P. Quantifying the impact of battery degradation and urban driving dynamics on the life cycle performance of electric vehicles: An energy, thermal, environmental, and economic analysis. *Energy Convers. Manag.* **2026**, *351*, 121021. https://doi.org/10.1016/j.enconman.2025.121021.
14. García, A.; Monsalve-Serrano, J.; Martinez-Boggio, S.; Golke, D. Energy assessment of the ageing phenomenon in Li-Ion batteries and its impact on the vehicle range efficiency. *Energy Convers. Manag.* **2023**, *276*, 116530. https://doi.org/10.1016/j.enconman.2022.116530.
15. Wang, Y.; Xu, C.; Chen, S.; Deng, Z.; Teng, Z. Dual-Metric-Driven Thermal–Fluid Coupling Modeling and Thermal Management Optimization for High-Speed Electric Multiple Unit Electrical Cabinets. *Energies* **2025**, *18*, 4693. https://doi.org/10.3390/en18174693.
16. Ma, J.; Liu, A.; Zhang, P.; Chen, Y.; Cai, Y. Collaborative thermal management of power battery and passenger cabin for energy efficiency optimization. *Energy Convers. Manag.* **2023**, *293*, 117514. https://doi.org/10.1016/j.enconman.2023.117514.
17. *DIN EN 14750:2025-02*; Railway Applications—Air Conditioning for Urban, Suburban and Regional Rolling Stock—Comfort Parameters and Type Tests; German version EN 14750:2024; DIN Media GmbH: Berlin, Germany, 2025.
18. *DIN EN 14750-1:2006-08*; Railway Applications—Air Conditioning for Urban and Suburban Rolling Stock—Part 1: Comfort Parameters; German version EN 14750-1:2006; DIN Media GmbH: Berlin, Germany, 2006.
19. *DIN EN 50591:2019-12;* Railway Applications—Rolling Stock—Specification and Verification of Energy Consumption; German version EN 50591:2019; DIN Media GmbH: Berlin, Germany, 2019.
20. Buonomano, A.; Forzano, C.; Giuzio, G.F.; Palombo, A.; Russo, G. Energy efficiency and indoor thermal comfort of railway carriages: Development of an innovative passenger-centric-control framework for HVAC systems. *Energy* **2024**, *307*, 132440. https://doi.org/10.1016/j.energy.2024.132440.
21. Barone, G.; Buonomano, A.; Forzano, C.; Giuzio, G.F.; Palombo, A.; Russo, G. An innovative waste heat recovery solution for HVAC systems in railway coaches: A path to enhanced energy efficiency. *Energy Rep.* **2025**, *13*, 5653–5661. https://doi.org/10.1016/j.egyr.2025.05.009.
22. González-Gil, A.; Palacin, R.; Batty, P.; Powell, J.P. A systems approach to reduce urban rail energy consumption. *Energy Convers. Manag.* **2014**, *80*, 509–524. https://doi.org/10.1016/j.enconman.2014.01.060.
23. Shao, Z.; Wang, Z.G.; Poredoš, P.; Ge, T.S.; Wang, R.Z. Highly efficient desiccant-coated heat exchanger-based heat pump to decarbonize rail transportation. *Energy* **2023**, *271*, 127014. https://doi.org/10.1016/j.energy.2023.127014.
24. Schmeling, D.; Zierke, O.; Maier, J.; Dehne, T.; Volkmann, A.; Marggraf-Micheel, C.; Goerke, P. Multi-jet personalized ventilation in passenger trains: Objective and subjective thermal comfort. *Build. Environ.* **2025**, *270*, 112510. https://doi.org/10.1016/j.buildenv.2024.112510.
25. Dullinger, C.; Struckl, W.; Kozek, M. Holistic energy simulation and optimization tool for urban rail vehicles. *Energy Convers. Manag.* **2018**, *174*, 101–111. https://doi.org/10.1016/j.enconman.2018.08.036.
26. Grden, L.; Škugor, B.; Deur, J.; Cvok, I. An Energy-Efficient Control Allocation Strategy for PTC Heater-Based Electric Vehicle Cabin Thermal Management. *Energies* **2026**, *19*, 1592. https://doi.org/10.3390/en19071592.
27. Boeck, L. Umweltfreundlichere Kältemittel für Bahn-Klimaanlagen—Wohin Geht Die Reise? (Engl. More Environmentally Friendly Refrigerants for Railway Air Conditioning Systems—Where is the Journey Headed?), 2023. Available online:

https://www.static.tu.berlin/fileadmin/www/10002264/ews/2022-wise/2023-01-16_EWS_Folien_Boeck_Umweltfreundlichere_Kaeltemittel_fuer_Bahn-Klimaanlagen.pdf (accessed on 21 July 2026).
28. Wieser, S.; Naveau, L.; Kraft, W.; Beristain, R.A.; Anson, A. Modeling and simulation of thermal management in battery electric rail vehicles for the sizing of thermal storage systems. *Energy Convers. Manag.* **2025**, *346*, 120489. https://doi.org/10.1016/j.enconman.2025.120489.
29. Seo, J.; Cha, J. Real-world analysis of energy consumption in a battery electric vehicle: Effects of ambient temperatures and thermal management system operation. *Energy Convers. Manag.* **2025**, *345*, 120372. https://doi.org/10.1016/j.enconman.2025.120372.
30. Trygstad, E. R744 HVAC Unit for NSB Flirt Trains, 2019. Available online: https://ntnuopen.ntnu.no/ntnu-xmlui/handle/11250/2454941 (accessed on 21 July 2026).
31. Han, X.; Zou, H.; Kang, W.; Xu, H.; Chen, Y.; Tian, C. Experimental investigation on vapor injection ASHP for electric rail vehicles in cold region. *Appl. Therm. Eng.* **2019**, *153*, 473–482. https://doi.org/10.1016/j.applthermaleng.2019.03.037.
32. Mastrullo, R.; Mauro, A.W.; Vellucci, C. Refrigerant Alternatives for High Speed Train A/C Systems: Energy Savings and Environmental Emissions Evaluation under Variable Ambient Conditions. *Energy Procedia* **2016**, *101*, 280–287. https://doi.org/10.1016/j.egypro.2016.11.036.
33. Sadjjadi, B.S.; Gerdes, J.-N.; Sauer, A. Energy flexible heat pumps in industrial energy systems: A review. *Energy Rep.* **2023**, *9*, 386–394. https://doi.org/10.1016/j.egyr.2022.12.110.
34. Liu, X.; Wang, D.; Guo, S.; Wang, G.; Li, H.; Chen, J. Investigation on the performance and vapor injection characteristics of a scroll compressor for electric vehicles based on computational fluid dynamics approach. *Energy Convers. Manag.* **2025**, *326*, 119419. https://doi.org/10.1016/j.enconman.2024.119419.
35. Yang, G.; Xiao, G.; Pan, C.; Wu, J.; Jia, Z. Control Strategy of the Vehicle Thermal Management System for Battery Electric Vehicles Considering Energy Consumption Optimization. *Energies* **2026**, *19*, 2687. https://doi.org/10.3390/en19112687.
36. Hao, S.; Han, K.; Wang, Y.; Liu, Q. Vapor compression cycle-based integrated thermal management systems for electric vehicles: A critical review. *Energy Convers. Manag.* **2024**, *321*, 119072. https://doi.org/10.1016/j.enconman.2024.119072.
37. Choi, H.; Kim, H.; Lee, S.; Choi, K.; Jung, Y.; Lee, H. Multi-objective design optimization of a CO2 gascooler for electric vehicle applications under all-climate conditions via the machine learning method. *Energy Convers. Manag.* **2026**, *350*, 120961. https://doi.org/10.1016/j.enconman.2025.120961.
38. González-Gil, A.; Palacin, R.; Batty, P. Optimal energy management of urban rail systems: Key performance indicators. *Energy Convers. Manag.* **2015**, *90*, 282–291. https://doi.org/10.1016/j.enconman.2014.11.035.
39. Donner, S.; Schenker, M.; Konrad, M.; Dittus, H.; Schindler, N. Shift2Rail FINE-2—Deliverable D4.3—Study on Potential Energy Savings by New Concepts and Smart Control of HVAC Systems, 2022. Available online: https://projects.shift2rail.org/download.aspx?id=75874bb6-a8c8-4b09-8946-1b0d5dbdade0 (accessed on 21 July 2026).
40. Xu, Z.; Zhao, N.; Yan, Y.; Gao, S.; Hillmansen, S. Electric-thermal collaborative system and control for hydrogen-fuel cell passenger trains in the UK's winter. *Energy Convers. Manag.* **2025**, *328*, 119629. https://doi.org/10.1016/j.enconman.2025.119629.
41. Zou, H.; Han, X.; Huang, G.; Chen, Y.; Tian, C. Analysis of Optimal Injection Ratio of Vapor Injection Heat Pump for Electric Railway Vehicles. *J. Sustain. Dev. Energy Water Environ. Syst.* **2019**, *7*, 656–666. https://doi.org/10.13044/j.sdewes.d7.0280.
42. Wang, C.; Wu, Q.; Zhang, J.; Zhao, Z.; Shi, H.; Wu, J. Enhancing ultra-low-temperature heat pump performance for high-speed trains using mechanism-based model. *Appl. Therm. Eng.* **2025**, *269*, 126021. https://doi.org/10.1016/j.applthermaleng.2025.126021.
43. Choi, J.; Park, J.; Ban, S.; Kim, K. Modeling the Impact of Ventilation Strategies on In-Cabin Air Quality and Energy Efficiency of the R744 Heat Pump. *Energies* **2026**, *19*, 119. https://doi.org/10.3390/en19010119.
44. Boeck, L.; Poser, S.; Mader, S.; Marschinke, A.; Danzer, P.; Claus, P.; Wegele, J.; Hörth, L.; Gschrey, B.; Warncke, K.; et al. Environmentally Friendly Mobile Air Conditioning with Natural Refrigerants: Air Conditioning of Rail Vehicles with Propane (R290), 2025. Available online: https://www.umweltbundesamt.de/publikationen/umweltfreundliche-mobile-klimatisierung (accessed on 21 July 2026).
45. Ernst, J. PINTA 3—Deliverable 8.3 HVAC Units with Natural Refrigerants, 2023. Available online: https://projects.shift2rail.org/download.aspx?id=ed08ea0c-6cdb-44fb-ac72-3a013dc1477d (accessed on 21 July 2026).
46. Aigner, R.; Kallinovsky, J.; Luger, C. Energy Efficiency Assessment of Natural Refrigerants in VCS HVAC for Rail Application. In Proceedings of the RTA-Workshop, Vienna, Austria, 16–17 June 2025.
47. European Union. Regulation (EU) 2024/573 of the European Parliament and of the Council of 7 February 2024 on Fluorinated Greenhouse Gases, Amending Directive (EU) 2019/1937 and Repealing Regulation (EU) No 517/2014, 2024. Available online: https://eur-lex.europa.eu/eli/reg/2024/573/oj/eng (accessed on 21 July 2026).

48. Ebinger, I.; Boeck, L. Natürliche Kältemittel in Klimaanlagen für Schienenfahrzeuge (engl. Natural refrigerants in air conditioning systems for rail vehicles). *EI Der Eisenbahningenieur* **2021**, *9/21*, 48–53.
49. Kwon, S.; Lee, D.; Ham, S.H.; Lee, M.; Kim, Y. Performance comparison of thermal management systems for electric vehicles using single- and dual-loop indirect heat pumps with propane. *Energy Convers. Manag.* **2025**, *327*, 119535. https://doi.org/10.1016/j.enconman.2025.119535.
50. Miao, Y.; Li, M.; Li, X.; Wang, J.; Qin, Z.; Tang, X. A reconfigurable dual-core R290 vehicular thermal management system featuring a variable area thermal unit: Experimental evaluation and thermodynamic analysis. *Energy Convers. Manag.* **2026**, *357*, 121452. https://doi.org/10.1016/j.enconman.2026.121452.
51. Pan, L.; Elmegaard, B.; Shi, W.; Zhou, J.; Kærn, M.R.; Markussen, W.B.; Wei, X. Theoretical investigation on a liquid-state pressurized carbon dioxide ejector heat pump cycle driven by waste heat. *Energy Convers. Manag.* **2026**, *348*, 120729. https://doi.org/10.1016/j.enconman.2025.120729.
52. Song, P.; An, Z.; Wei, M.; Sun, X.; Zhao, Y.; Dan, D.; Zhang, Y. Cooling performance and optimization of a thermal management system based on CO2 heat pump for electric vehicles. *Energy Convers. Manag.* **2024**, *306*, 118299. https://doi.org/10.1016/j.enconman.2024.118299.
53. Zhang, T.; Cao, F.; Song, Y.; Ren, J.; Bai, G.; Pang, X.; He, Y. The model predictive control strategy of the transcritical CO_2 air conditioning system used in railway vehicles. *Appl. Therm. Eng.* **2023**, *218*, 119376. https://doi.org/10.1016/j.applthermaleng.2022.119376.
54. Jiang, L.; Song, Y.; Chen, Y.; Xie, H.; Ren, J.; Yin, X.; Cao, F.; Pang, X.; Bai, G.; Yang, T.; et al. The performance improvement and optimum control of the transcritical CO_2 air conditioning and heat pump system used in the high-speed railway vehicles. *Int. J. Refrig.* **2026**, *182*, 49–60. https://doi.org/10.1016/j.ijrefrig.2025.11.009.
55. Zhang, Y.; Song, C.; Zang, J.; Chen, X.; Lu, C. Study on the Replacement of Rail Vehicle Air-Conditioning Refrigerants with Low-GWP Refrigerant Mixtures. *Energies* **2025**, *18*, 5164. https://doi.org/10.3390/en18195164.
56. Kwon, M.; Yun, R.; Kim, H. Design of heat pump system for a railway train's cabin applications utilizing R744 and R290. *Int. J. Air-Cond. Ref.* **2025**, *33*, 21. https://doi.org/10.1007/s44189-025-00082-2.
57. Aigner, R.; Krawanja, A.; Luger, C.; Wollweber, M.; Claus, P.; Hörth, L.; Streng, M. Umweltfreundliche Klimatisierung Von Zügen: Felddatenmessung Und-Auswertung an Luftgestützter Klimaanlage am ICE 3 (Engl. Environmentally Friendly Air Conditioning for Trains: Field Data Measurement and Evaluation on Air-Based Air Conditioning System on ICE 3), 2019. Available online: https://www.umweltbundesamt.de/en/publikationen/umweltfreundliche-klimatisierung-von-zuegen (accessed on 21 July 2026).
58. Schenker, M.; Wieser, S.; Moser, I.; Böhm, M. Holistic Modeling and Optimization of Hydrogen-Powered Trains for Zero-Emission Railway Operation, 2025. Available online: https://elib.dlr.de/220972/ (accessed on 21 July 2026).
59. Bell, I.H.; Wronski, J.; Quoilin, S.; Lemort, V. Pure and Pseudo-pure Fluid Thermophysical Property Evaluation and the Open-Source Thermophysical Property Library CoolProp. *Ind. Eng. Chem. Res.* **2014**, *53*, 2498–2508. https://doi.org/10.1021/ie4033999.
60. *DIN EN 13129:2016-12*; Railway Applications—Air Conditioning for Main Line Rolling Stock—Comfort Parameters and Type Tests; German version EN 13129:2016; DIN Media GmbH: Berlin, Germany, 2016.
61. Minas. MapChart, 2026. Available online: https://www.mapchart.net (accessed on 21 July 2026).